Cyclotron Resonance Experiments in Uniaxially Stressed Silicon: Valence Band Inverse Mass Parameters and Deformation Potentials

J. C. HENSEL
Bell Telephone Laboratories, Murray Hill, New Jersey

AND

G. FEHER*
University of California, LaJolla, California

(Received 28 August 1962)

Cyclotron resonance of holes in unstressed or "cubic" silicon fails to specify uniquely the valence band parameters because of the complex shape of the warped energy surfaces. The application of uniaxial stresses to the crystal lifts the cubic symmetry and removes the degeneracy at $\mathbf{k}=0$ of the valence band which is responsible for the warping of the surfaces. The ellipsoidal energy surfaces of the decoupled bands give cyclotron resonance masses amenable to simple interpretation. From the measured masses (at 1.26°K and ~9000 Mc/sec) the following quantities have been determined: the inverse mass band parameters (in units of $\hbar^2/2m_0$) $A=-4.28\pm0.02$, $|B|=0.75\pm0.04$, and $|N|=9.36\pm0.10$; the absolute value of the ratio of the band splitting deformation potentials $|D_u'/D_u|=1.31\pm0.03$; and the signs of the quantities $BD_u<0$ and $ND_u'<0$. The interaction of the spin-orbit split-off band with the valence band edge under strain allows the signs and magnitudes of the deformation potentials to be obtained. They are $D_u=+(2.04\pm0.20)$ eV and $D_u'=+(2.68\pm0.25)$ eV. The results indicate that the $M_J=\pm1/2$ band moves "up" and the $M_J=\pm3/2$ band "descends" under compressive stresses along the [001] and [111] crystallographic axes. This fact in conjunction with the ratio of deformation potentials shows that the quantization and band energy splitting are approximately isotropic with respect to the direction of stress. Finally, the signs of B and N were determined to be *negative*, the negative sign of B being contrary to that predicted by band theory. An investigation of the shape of the split-band hole resonance confirms the line-broadening mechanism proposed by Hasegawa.

I. INTRODUCTION

At low temperatures, free holes and electrons in a semiconductor crystal in an external magnetic field H_0 can execute orbital or cyclotron motion[1] at an angular frequency $\omega_c=eH_0/m^*c$, where m^* is the effective mass of the charge carriers. Since the effective mass is a measure of the curvature of the bands, the cyclotron resonance determines the shape of the energy surfaces near the band edges. This technique has been used extensively in exploring the band structure of silicon and germanium.[2] Significant features of the valence bands have, however, remained obscure. The present investigation was undertaken in an attempt to shed further light on these matters by a study of the cyclotron resonance of holes in silicon single crystals elastically deformed by the application of large, uniaxial stresses.

From the early cyclotron resonance experiments[3,4] it was evident that the energy surfaces belonging to the valence band edge for silicon are considerably more complex than those for the conduction bands. The latter have ellipsoidal energy surfaces for which a measurement of the anisotropy of the effective mass m^* is sufficient to define the mass tensor. The situation for the degenerate valence band edge at $\mathbf{k}=0$ is quite another matter. Coupling between the degenerate bands distorts the energy surfaces into quartic surfaces, often called "warped" or "fluted." These warped energy surfaces, which cannot be represented by a mass tensor, are usually described in terms of the so-called inverse mass band parameters[3] A, B, and N. Cyclotron resonance on complex surfaces of this type suffers from two major drawbacks. First of all, the warping severely broadens and shifts the resonance lines making it difficult to locate their true centers accurately. A second and more fundamental limitation is the fact that the measurements fail to specify the signs of two of the band parameters B and N, since the shape of the energy surfaces is independent of these signs.

This experimental ambiguity is indeed unfortunate for silicon because a controversy has existed over the sign of B which is especially important since it is sensitive to the ordering of the conduction bands at $\mathbf{k}=0$. (A negative sign implies a germanium-like band structure.) In their original paper, Dresselhaus, Kip, and Kittel[3] proposed a positive sign for B which was supported by more recent band calculations of Kleinman and Phillips.[5] Theoretical arguments by Kane,[6] on the other hand, favored the negative sign. In view of this uncertainty, an experimental determination of the sign of B seemed highly desirable.

The shortcomings of "classical" microwave cyclotron

* Work performed at Bell Telephone Laboratories, Murray Hill, New Jersey.

[1] J. Dorfmann, Doklady Akad. Nauk S.S.S.R. **81**, 765 (1951); R. B. Dingle, Ph.D. thesis, Cambridge University, 1951 (unpublished); *Proceedings of the International Conference on Very Low Temperatures* (Oxford University Press, New York, 1951), p. 165; Proc. Roy. Soc. (London) **A212**, 38 (1952); W. Shockley, Phys. Rev. **90**, 491 (1953).

[2] For a review on this subject see B. Lax and J. G. Mavroides, in *Solid State Physics*, edited by F. Seitz and D. Turnbull (Academic Press Inc., New York, 1960), Vol. 11, p. 261.

[3] G. Dresselhaus, A. F. Kip, and C. Kittel, Phys. Rev. **98**, 368 (1955).

[4] R. N. Dexter, H. J. Zeiger, and B. Lax, Phys. Rev. **104**, 637 (1956).

[5] L. Kleinman and J. C. Phillips, Phys. Rev. **118**, 1153 (1960).

[6] E. O. Kane, J. Phys. Chem. Solids **1**, 83 (1956).

resonance experiments in the valence bands can in principle be circumvented by the detailed analysis of the quantum cyclotron resonance spectrum[7,8] seen at mm wavelengths. This consists of numerous weak lines that originate from transitions between the anomalously spaced, low-lying Landau levels. Although the interpretation of the quantum lines near 1°K, no doubt, provides the most comprehensive picture of the valence band structure, the analysis of the spectra is sufficiently complicated to require a fairly accurate set of "trial values" for the band parameters. One of the objectives of this work is to obtain them to a higher degree of accuracy.

The present study constitutes an alternative approach to the problem based on recent theoretical investigations[9,10] of the effects of uniaxial stress upon the degenerate valence bands. Uniaxial stress on the crystal lifts the cubic symmetry and removes the degeneracy at $\mathbf{k}=0$ responsible for the warping of the energy surfaces. In zero magnetic field the decoupled states are degenerate Kramers' doublets identified by the magnetic quantum number $\pm M_J$ for stress along the [001] and [111] directions. The decoupled bands have ellipsoidal energy surfaces which—like the conduction bands—give cyclotron resonance masses amenable to straightforward interpretation. Preliminary measurements[11] on germanium and silicon have indeed confirmed the predicted effects upon the cyclotron resonance spectrum.

As is shown in detail in Sec. II, for uniaxial stresses along each of the three principal crystallographic directions [001], [111], and [110] the mass tensor of the ellipsoids is related in an elementary way to the original band parameters A, B, and N. Thus, from measurements of cyclotron masses in Si the following have been determined: the inverse mass band parameters A, $|B|$, and $|N|$; the absolute value of the ratio of the band splitting deformation potentials[12] D_u and D_u'; and the signs of the quantities BD_u and ND_u'. The signs of B and N enter the analysis only through the products BD_u and ND_u'. Since little information is available concerning D_u and D_u', one needs to ascertain their signs from a different type of measurement.

Some evidence bearing on this point is available from the spin-resonance experiments[13] of acceptor states in silicon under compressive stress. It is preferable, however, to have confirmation of the sign of D_u and D_u' from direct measurements on the band edge itself. Such information can be derived from the observation[14] that the effective masses shift linearly with increasing stress. Hasegawa[10] has recently shown that such shifts arise from a strain-induced admixture of the spin-orbit split-off valence band with *one* of the upper valence bands. The presence or absence of the shift for the observed cyclotron line determines the character assignment of the topmost band fixing the sign of D_u or D_u' and, in turn, the sign for B or N. The magnitude of D_u and D_u' has also been obtained from measurements of the mass shifts.

In connection with the deformation potentials, we arrive at a rather surprising conclusion. The results indicate that the $M_J=\pm\frac{1}{2}$ band moves "up" and the $M_J=\pm\frac{3}{2}$ band moves "down" under compressive stresses along the [001] and [111] crystallographic axes. This fact, in conjunction with the ratio of deformation potentials, shows that the band energy splitting is nearly isotropic with respect to the direction of stress. Furthermore, this is the condition for isotropic quantization, i.e., that $\pm M_J$ is nearly a good quantum number for arbitrary stress direction.

The shape of the hole resonance line exhibits several striking features. It is asymmetric with a tail on the high mass side. Its linewidth is not simply determined by the hole scattering relaxation time, but has been shown by Hasegawa to arise from an uneven spacing of the Landau levels. Hasegawa's theory for the line broadening was experimentally checked and verified in detail.

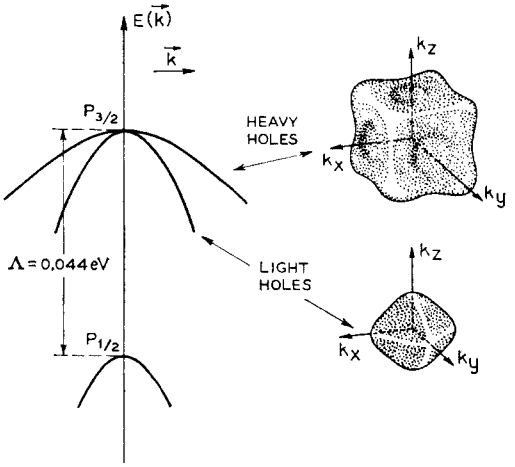

FIG. 1. The valence bands of "cubic" silicon near $\mathbf{k}=0$. The warped energy surfaces of the light- and heavy-hole bands are shown schematically. The spin-orbit split-off band labeled by its spectroscopic character $p_{1/2}$ has spherical energy surfaces which are not shown.

[7] R. C. Fletcher, W. A. Yager, and F. R. Merritt, Phys. Rev. **100**, 747 (1955); J. C. Hensel, Bull. Am. Phys. Soc. **6**, 115 (1961); J. J. Stickler, C. Rauch, H. J. Zeiger, and G. S. Heller, *ibid.* **6**, 115 (1961).

[8] J. M. Luttinger, Phys. Rev. **102**, 1030 (1956).

[9] G. E. Pikus and G. L. Bir, Fiz. Tverd. Tela, **1**, 154, 1642 (1959); **3**, 1001 (1961) [translations: Soviet Phys.—Solid State **1**, 136, 1502 (1959); **3**, 730 (1961)]; Phys. Rev. Letters **6**, 103 (1961). We would like to express our regrets of having omitted references to the work of G. E. Pikus and G. L. Bir in our earlier communication (reference 11).

[10] H. Hasegawa, preceding paper [Phys. Rev. **129**, 1029 (1963)].

[11] J. C. Hensel and G. Feher, Phys. Rev. Letters **5**, 307 (1960).

[12] W. H. Kleiner and L. M. Roth, Phys. Rev. Letters **2**, 334 (1959).

[13] G. Feher, J. C. Hensel, and E. A. Gere, Phys. Rev. Letters **5**, 309 (1960).

[14] J. C. Hensel, Bull. Am. Phys. Soc. **6**, 304 (1961).

II. VALENCE BANDS OF SILICON NEAR $k=0$

A. In the Absence of Strain

Without strain or spin-orbit splitting the valence band edge of silicon is a sixfold degenerate p multiplet characterized by symmetry $\Gamma_{25'}$ of the cubic group. The sixfold multiplet is comprised of three bands each twofold degenerate due to spin. In the vicinity of $\mathbf{k}=0$, the shapes of the bands can be determined using $\mathbf{k}\cdot\mathbf{p}$ perturbation theory ($\mathbf{p}$=momentum operator). The perturbation matrix[3] in $(m_l m_s)$ representation is

$$\mathcal{H}(m_s=\pm\tfrac{1}{2})=\begin{vmatrix} Lk_x^2+M(k_y^2+k_z^2) & Nk_xk_y & Nk_xk_z \\ Nk_yk_x & Lk_y^2+M(k_x^2+k_z^2) & Nk_yk_z \\ Nk_zk_x & Nk_zk_y & Lk_z^2+M(k_x^2+k_y^2) \end{vmatrix}, \tag{1}$$

where

$$\begin{aligned} L&=F+2G,\\ M&=H_1+H_2,\\ N&=F-G+H_1-H_2. \end{aligned} \tag{2}$$

The band parameters F, G, H_1, and H_2 correspond to the individual contributions from each of the four representations that can perturb the valence band edge as classified in Table I.[5,15,16]

Actually for silicon the spin-orbit interaction partially lifts the degeneracy at $\mathbf{k}=0$. The sixfold degenerate p state splits into a fourfold $p_{3/2}$ multiplet and a twofold $p_{1/2}$ multiplet with separation[17] $\Lambda=0.044$ eV (see Fig. 1). The band edge, the upper $J=3/2$ state, consists now of a pair or twofold degenerate bands usually designated as the "light" and "heavy" hole bands. Off $\mathbf{k}=0$, the energy surfaces can be determined, as before, by the $\mathbf{k}\cdot\mathbf{p}$ perturbation technique. A generalization [in (JM_J) representation] of (1) including the spin-orbit interaction can be diagonalized to give the energy surfaces for the $J=3/2$ band[3]

$$E(k)=Ak^2\pm[B^2k^4+C^2(k_x^2k_y^2+k_x^2k_z^2+k_y^2k_z^2)]^{1/2}, \tag{3}$$

where the inverse mass band parameters A, B, and C are defined by

$$\begin{aligned} A&=\tfrac{1}{3}(L+2M)+\hbar^2/2m_0,\\ B&=\tfrac{1}{3}(L-M),\\ C^2&=\tfrac{1}{3}[N^2-(L-M)^2]. \end{aligned} \tag{4}$$

The upper and lower choices of signs in (3) refer, respectively, to the heavy and light holes. The shapes of the energy surfaces are pictured in Fig. 1. The coupling between the light- and heavy-hole bands via the degeneracy at $\mathbf{k}=0$ is responsible for the warped or fluted form of the energy surfaces.

The lower $J=\frac{1}{2}$ band has spherical energy surfaces given by

$$E(k)=Ak^2-\Lambda. \tag{5}$$

Cyclotron resonance absorption has not been observed for this band.

The interpretation of cyclotron resonance measurements in the $J=\frac{3}{2}$ bands is difficult for the following reasons:

(a) Since B and N enter (3) quadratically, it is impossible to determine their signs from the shape of the energy surfaces or, equivalently, from the cyclotron resonance spectrum. The importance of the signs, especially for B, has been emphasized earlier.

(b) Quantum effects arise at low temperatures which, even though unresolved at X- or K-band frequencies, can shift the apparent line center.

(c) In the analysis leading to Eq. (3) the coupling between the $J=\frac{3}{2}$ and $J=\frac{1}{2}$ bands was ignored. For silicon with a small spin-orbit separation of $\Lambda=0.044$ eV this assumption may contribute errors in the application of (3) to cyclotron resonance.

(d) From an experimental point of view the most serious consequence of the warping is the k_z broadening which spreads and shifts the lines in a complicated way. The mechanism for k_z broadening is quite simple. On a complex energy surface, orbits of different k_z (a constant of motion for z axis chosen along H_0) have different periods. With carriers distributed thermally over all allowed values of k_z, the resultant cyclotron line is a composite of many such individual lines. Reasonably accurate calculations to correct for the k_z broadening and shifts are exceedingly hard to make.

In view of these drawbacks it is expedient to consider new methods of tackling the valence band problem. One approach involving uniaxial stresses is discussed next.

TABLE I. Tabulation of the irreducible representations which perturb the valence band edge.

Band parameter	Irreducible representation	Atomic character	Conduction band energy (measured from $\Gamma_{25'}$)
F	$\Gamma_{2'}$	Antibonding s	$\sim$3 eV[a]
G	$\Gamma_{12'}$	Antibonding d	$\sim$10 eV[b]
H_1	Γ_{15}	Antibonding p	$\sim$3.4 eV[a]
H_2	Γ_{25}	Antibonding d	$\sim$30 eV[b]

[a] Extrapolated from optical absorption measurements in Ge-Si alloys See references 15 and 16.
[b] Estimated from band theory. See references 5 and 16.

[15] J. Tauc and A. Abraham, *Proceedings of the International Conference in Semiconductor Physics, Prague, 1960* (Czechoslovakian Academy of Sciences, Prague, 1961), p. 375; J. Tauc and A. Abraham, J. Phys. Chem. Solids **20**, 190 (1961).
[16] J. C. Phillips, Phys. Rev. **125**, 1931 (1962).
[17] S. Zwerdling, K. J. Button, B. Lax, and L. M. Roth, Phys. Rev. Letters **4**, 173 (1960).

B. In the Presence of Strain

A uniaxial stress applied to a silicon crystal removes the cubic symmetry; and the $J=\frac{3}{2}$ valence band splits further into a pair of degenerate Kramers' doublets. Under special conditions these may be identified by the magnetic quantum number $\pm M_J$. Kleiner and Roth[12] have constructed a strain Hamiltonian in terms of the angular momentum operator $\mathbf{J}(J=\frac{3}{2})$ to describe the splitting of the $p_{3/2}$ states at $\mathbf{k}=0$,

$$\begin{aligned}H_e=&D_d^v(e_{xx}+e_{yy}+e_{zz})+\tfrac{2}{3}D_u[(J_x^2-\tfrac{1}{3}J^2)e_{xx}\\&+(J_y^2-\tfrac{1}{3}J^2)e_{yy}+(J_z^2-\tfrac{1}{3}J^2)e_{zz}]\\&+\tfrac{2}{3}D_u'[\{J_xJ_y\}e_{xy}+\{J_xJ_z\}e_{xz}+\{J_yJ_z\}e_{yz}],\end{aligned}\quad(6)$$

where e_{xx}, $\cdots$, e_{xy}, $\cdots$, are the "conventional" strain components (see Appendix A) and D_d^v, D_u, and D_u' are the valence band deformation potentials.[18] D_u^v gives the shift of the center of gravity of the entire valence band. It does not, however, contribute to the splitting and is henceforth ignored. D_u and D_u' define the valence band splitting for uniaxial stress along the [001] and [111] directions, respectively. The factors $\{J_xJ_y\}$, etc., represent the symmetrized products, i.e., $\{J_xJ_y\}=\frac{1}{2}(J_xJ_y+J_yJ_x)$.

To determine the shapes of the $J=\frac{3}{2}$ bands off $\mathbf{k}=0$ there must be added to H_e in (6) the Hamiltonian[8] for the $\mathbf{k}\cdot\mathbf{p}$ perturbation

$$\begin{aligned}H_k=&A(k_x^2+k_y^2+k_z^2)-B[k_x^2(J_x^2-\tfrac{1}{3}J^2)\\&+k_y^2(J_y^2-\tfrac{1}{3}J^2)+k_z^2(J_z^2-\tfrac{1}{3}J^2)]\\&-(2N/3)[\{k_xk_y\}\{J_xJ_y\}+\{k_xk_z\}\{J_xJ_z\}\\&+\{k_yk_z\}\{J_yJ_z\}]\end{aligned}\quad(7)$$

and the sum $H_0=H_e+H_k$ must be diagonalized. We consider the special cases for the stress T along the principal crystallographic directions. A general solution for any orientation of T in the $(1\bar{1}0)$ plane is given in Appendix B.

(1) *Stress Parallel to [001]: Tetragonal Distortions*

For $T\|[001]$ the strain components (see Appendix A) are

$$\begin{aligned}&e_{xx}=e_{yy}=s_{12}T,\\&e_{zz}=s_{11}T,\\&e_{xy}=e_{xz}=e_{yz}=0,\end{aligned}\quad(8)$$

where s_{11} and s_{12} are cubic compliance constants. The splitting Hamiltonian (6) thus becomes

$$H_e=\tfrac{2}{3}D_u(s_{11}-s_{12})T(J_z^2-\tfrac{1}{3}J^2),\quad(9)$$

which is diagonal with the $M_J=+\frac{3}{2}$ states split from the $M_J=\pm\frac{1}{2}$ states. The remaining twofold, Kramers' degeneracy of each state can be lifted only by application of a magnetic field. The fact that $\pm M_J$ is a good quantum number is a consequence of the choice of the axis of quantization along the stress direction. The eigenvalues of (9) are the band energies at $\mathbf{k}=0$

$$\begin{aligned}&E_{3/2}=+\epsilon_0,\\&E_{1/2}=-\epsilon_0,\end{aligned}\quad(10)$$

where

$$\epsilon_0=\tfrac{2}{3}D_uS\quad\text{and}\quad S=(s_{11}-s_{12})T.$$

Under large strains the valence bands decouple so that H_k can be considered a first-order perturbation. Therefore, to lowest order in k the eigenvalues of the total Hamiltonian H_0 are the diagonal elements[19]

$$\begin{aligned}&E_{3/2}(k)=(A+\tfrac{1}{2}B)k_\perp^2+(A-B)k_{||}^2+\epsilon_0,\\&E_{1/2}(k)=(A-\tfrac{1}{2}B)k_\perp^2+(A+B)k_{||}^2-\epsilon_0,\end{aligned}\quad(11)$$

where

$$k_\perp^2=k_x^2+k_y^2\quad\text{and}\quad k_{||}^2=k_z^2.$$

Thus, the energy surfaces near $\mathbf{k}=0$ become ellipsoids of revolution, one prolate and the other oblate, whose axis of symmetry is along the stress direction as shown in Fig. 2. Examination of (11) reveals that $E_{3/2}(k)\rightarrow E_{1/2}(k)$ under the transformation $B\rightarrow -B$ and $\epsilon_0\rightarrow-\epsilon_0$; so at best we can determine only the sign of the product ϵ_0B. We can, however, re-express Eq. (11) in the invariant form

$$E_\pm(k)=\left(A\pm\tfrac{1}{2}B\frac{\epsilon_0}{|\epsilon_0|}\right)k_\perp^2+\left(A\mp B\frac{\epsilon_0}{|\epsilon_0|}\right)k_{||}^2\pm|\epsilon_0|,\quad(12)$$

where the upper and lower signs refer, respectively, to the top $+|\epsilon_0|$ and bottom $-|\epsilon_0|$ bands. A measurement of the effective masses for the top band $+|\epsilon_0|$ with $T\|[001]$ determines, according to Eq. (12) the values of A, $|B|$, and the sign of ϵ_0B. The lower band $-|\epsilon_0|$ is depopulated at liquid He temperatures and is not observed by cyclotron resonance.

(2) *Stress Parallel to [111]: Trigonal Distortions*

For $T\|[111]$ the analysis is nearly identical to that for [001] case. The strain components are (see Appendix A)

$$\begin{aligned}&e_{xx}=e_{yy}=e_{zz}=(s_{11}+2s_{12})\tfrac{1}{3}\mathrm{T},\\&e_{xy}=e_{xz}=e_{yz}=s_{44}\tfrac{1}{3}T\end{aligned}\quad(13)$$

where s_{44} is a cubic elastic compliance constant. The splitting Hamiltonian (6) becomes

$$H_e=\tfrac{2}{3}D_u's_{44}(T/3)[\{J_xJ_y\}+\text{cycl. perm.}].\quad(14)$$

At this point the problem becomes straightforward if we rotate $\mathbf{J}$ so that $(J_x,J_y,J_z)\rightarrow(J_1,J_2,J_3)$ with J_3 diagonal along the [111] direction. (The choice of the perpendicular axes J_1 and J_2 is immaterial.) Making

[18] See reference 12. The Kleiner-Roth definitions of the deformation potentials are related to Pikus and Bir's notation by $D_d^v=-\frac{3}{2}a$, $D_u=-\frac{3}{2}b$, $D_{u'}=-\frac{1}{2}\sqrt{3}d$.

[19] Strictly speaking, the error in such a procedure will be of order k^4/ϵ_0. The effects of these fourth-order terms have been investigated in detail by H. Hasegawa (reference 10).

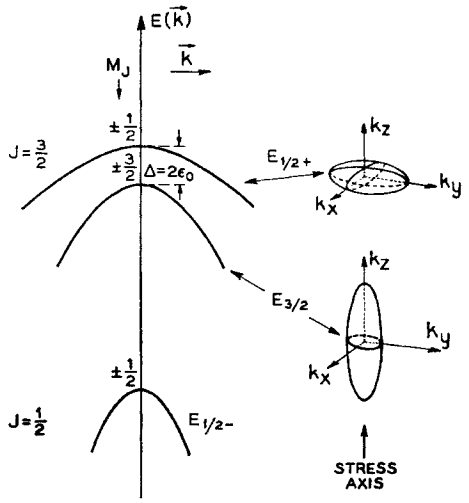

FIG. 2. The split valence bands of uniaxially stressed silicon. The band splitting at $\mathbf{k}=0$, denoted by Δ, is shown for a compressive stress $T\|[001]$. For a uniaxial tension the ordering of the bands would be reversed from that shown. The energy surfaces near $\mathbf{k}=0$ are a prolate ellipsoid and an oblate ellipsoid both having axial symmetry about T (k_z axis).

such a transformation we obtain

$$H_e=\tfrac{2}{3}D_u'(s_{44}/2)T[J_3^2-\tfrac{1}{3}J^2] \tag{15}$$

similar to the previous result (9). H_e, now diagonal for the axis of quantization along the [111] direction, has the eigenvalues[20]

$$\begin{aligned} E_{3/2}&=+\epsilon_0' \\ E_{1/2}&=-\epsilon_0', \end{aligned} \tag{16}$$

where

$$\epsilon_0'=\tfrac{2}{3}D_u'S' \quad \text{and} \quad S'=(s_{44}/2)T.$$

Next, after transforming H_k so that k_3 and J_3 are both along [111], we find the eigenvalues of H_0 (transformed) to lowest order in k,

$$\begin{aligned} E_{3/2}(k)&=(A+\tfrac{1}{6}N)k_\perp^2+(A-\tfrac{1}{3}N)k_{11}^2+\epsilon_0', \\ E_{1/2}(k)&=(A-\tfrac{1}{6}N)k_\perp^2+(A+\tfrac{1}{3}N)k_{11}^2-\epsilon_0', \end{aligned} \tag{17}$$

where

$$k_\perp^2=k_1^2+k_2^2 \quad \text{and} \quad k_{11}^2=k_3^2.$$

This can be again rewritten as

$$E_\pm(k)=\left(A\pm\frac{N\epsilon_0'}{6|\epsilon_0'|}\right)k_\perp^2+\left(A\mp\frac{N\epsilon_0'}{3|\epsilon_0'|}\right)k_{11}^2\pm|\epsilon_0'| \tag{18}$$

for the upper $+|\epsilon_0'|$ and lower $-|\epsilon_0'|$ bands. Thus, for $T\|[111]$ we can determine A, $|N|$, and the sign of $\epsilon_0'N$.

(3) *Stress Parallel to [110]: Orthorhombic Distortions*

In the previous two examples, $T\|[001]$ and $T\|[111]$, we discovered that a judicious choice of the quantization axis along T led to simple and easily interpretable results. Most significantly, the split states could be identified by the magnetic quantum number $\pm M_J$ and the energy surfaces are elliposids of revolution with the principal symmetry axis along the stress direction. Both are consequences of the high order of rotational symmetry about the [001] and [111] directions (fourfold and threefold, respectively). However, when T is along an axis of lower symmetry such as the twofold [110], the situation is substantially more complicated.

The strain components for $T\|[110]$ are (see Appendix A)

$$\begin{aligned} e_{xx}&=e_{yy}=(s_{11}+s_{12})\frac{T}{2}, \\ e_{zz}&=s_{12}T, \\ e_{xy}&=s_{44}\frac{T}{2}, \\ e_{xz}&=e_{yz}=0, \end{aligned} \tag{19}$$

for which the splitting Hamiltonian (6) becomes

$$\begin{aligned} H_e=&-\tfrac{2}{3}D_u(T/2)(s_{11}-s_{12})(J_z^2-\tfrac{1}{3}J^2) \\ &+\tfrac{2}{3}D_u'(T/2)s_{44}\{J_xJ_y\}. \end{aligned} \tag{20}$$

If we rotate $\mathbf{J}$ according to the transformation

$$\begin{aligned} J_x&=(1/\sqrt{2})(J_1+J_3), \\ J_y&=(1/\sqrt{2})(-J_1+J_3), \\ J_z&=-J_2, \end{aligned} \tag{21}$$

with J_3 diagonal to quantize along the [110] direction then

$$\begin{aligned} H_e=&-\tfrac{2}{3}D_u(T/2)(s_{11}-s_{12})(J_2^2-\tfrac{1}{3}J^2) \\ &+\tfrac{2}{3}D_u'(s_{44}/2)(T/2)(J_3^2-J_1^2). \end{aligned} \tag{22}$$

As it stands this is not diagonal, so $\pm M_J$ is not a good quantum number and, in general, the strain split states consist of mixtures of the basis functions for $M_J=\pm\frac{3}{2}$, $\pm\frac{1}{2}$. Under special conditions, however, H_e becomes diagonal and the system then regains the "uniaxial" property for the [110] direction as well. We can see this easily by going to a matrix representation[21] for H_e giving

$$H_e=\tfrac{1}{4}\begin{bmatrix} (\epsilon_0+3\epsilon_0') & 0 & \sqrt{3}(\epsilon_0'-\epsilon_0) & 0 \\ 0 & -(\epsilon_0+3\epsilon_0') & 0 & \sqrt{3}(\epsilon_0'-\epsilon_0) \\ \sqrt{3}(\epsilon_0'-\epsilon_0) & 0 & -(\epsilon_0+3\epsilon_0') & 0 \\ 0 & \sqrt{3}(\epsilon_0'-\epsilon_0) & 0 & (\epsilon_0+3\epsilon_0') \end{bmatrix}, \tag{23}$$

[20] The splitting energy for $T\|[111]$ quoted earlier (reference 11) is incorrect by a factor $\frac{1}{2}$. The origin of the discrepancy is fully discussed in Appendix A. We are indebted to S. Koenig for bringing this error to our attention.

[21] See Eq. (39) of reference 8.

in terms of the splitting energies ϵ_0 and ϵ_0' introduced earlier. Clearly from (23) we see that H_e becomes diagonal when $\epsilon_0=\epsilon_0'$, the case of equal band splitting under equal applied stresses along the [111] and [001] directions. Indeed, when $\epsilon_0=\epsilon_0'$ the band splitting becomes isotropic, and H_e is diagonal for any orientation of T—the condition for "isotropic quantization."[10] We later see that such is approximately the situation for silicon.

To calculate the effective masses for $T\|[110]$ we make use of the general solutions (setting $\theta=90°$) in Appendix B. The k's have been transformed, so that k_1, k_2, and k_3 are along the $[1\bar{1}0]$, $[00\bar{1}]$, and [110] directions, respectively. In this scheme the energy surfaces are

$$E_\pm(k)=\frac{\hbar^2}{2m_1}k_1^2+\frac{\hbar^2}{2m_2}k_2^2+\frac{\hbar^2}{2m_3}k_3^2\pm\tfrac{1}{2}(\epsilon_0^2+3\epsilon_0'^2)^{1/2}, \quad (24)$$

where the inverse effective masses are given by

$$\begin{aligned}\frac{\hbar^2}{2m_1}&=A\mp\tfrac{1}{2}B\frac{\epsilon_0}{|\epsilon_0|}\eta_1\pm\tfrac{1}{2}N\frac{\epsilon_0'}{|\epsilon_0'|}\eta_2,\\ \frac{\hbar^2}{2m_2}&=A\pm B\frac{\epsilon_0}{|\epsilon_0|}\eta_1,\\ \frac{\hbar^2}{2m_3}&=A\mp\tfrac{1}{2}B\frac{\epsilon_0}{|\epsilon_0|}\eta_1\mp\tfrac{1}{2}N\frac{\epsilon_0'}{|\epsilon_0'|}\eta_2,\end{aligned} \quad (25)$$

with

$$\eta_1=\left(\frac{1}{1+3\beta^2}\right)^{1/2}, \quad \eta_2=\left(\frac{\beta^2}{1+3\beta^2}\right)^{1/2},$$

and $\beta=\epsilon_0'/\epsilon_0$ is the splitting anisotropy parameter. The energy surfaces are now ellipsoids of the most general form with three unequal principal axies and without a symmetry axis of revolution. One new feature of the $T\|[110]$ case is the appearance of the parameter β in the effective masses. Measurements of m_1, m_2, and m_3 determine, therefore, the ratio of the absolute values of the deformation potentials D_u and D_u' in addition to the band parameters. A stress in a direction other than the three principal directions gives essentially no further information. The determination of the signs of D_u and D_u', as we see in the next section, must come from considerations of the interaction of the $J=\frac{3}{2}$ multiplet with other nearby bands.

C. Mass Shifts due to Higher Order Effects

So far we have ignored the influence of the nearby $J=\frac{1}{2}$ split-off band, labeled henceforth $E_{1/2}^-$, upon the top $J=\frac{3}{2}$ multiplet. Furthermore, in our discussion it has been assumed that the $J=\frac{3}{2}$ state is completely decoupled by strain into two doublets, $E_{3/2}$ and $E_{1/2}^+$ whose energy bands are parabolic near $\mathbf{k}=0$. In practice, however, neither assumption is strictly justified. Recently, Hasegawa[10] has shown that the breakdown of each approximation leads to a characteristic "mass shift" of the split-band cyclotron line with stress. Here we outline his conclusions pertinent to the interpretation of the experimental results to follow.

(1) *Linear Mass Shift due to Valence Band Mixing*

When the cubic crystal is stressed uniaxially, the spherical isotropy imposed by the spin-orbit interaction is lifted so that J is no longer a good quantum number, and the strain admixes the $J=\frac{3}{2}$ and $J=\frac{1}{2}$ eigenstates. This admixture, ordinarily forbidden for cubic silicon when $T=0$, gives rise to a *linear* effective mass shift with stress. For the important case of "uniaxial" distortions $\pm M_J$ is still a good quantum number, and mixing, therefore, can take place only between states having the same $\pm M_J$, i.e., only between $E_{1/2}^+$ and $E_{1/2}^-$. This important property permits identification of the character of the members of the $J=\frac{3}{2}$ band—the observation of a linear mass shift implies the "top" member of the $J=\frac{3}{2}$ multiplet is $E_{1/2}^+$.

To first order in ϵ_0/Λ Hasegawa finds the inverse effective mass of the $E_{1/2}^+$ band is shifted by an amount αT, where α is an anisotropic constant given as follows:

$T\|[001]$

$$\begin{aligned}\Delta(1/m_\perp)&=\alpha_\perp T=2B\epsilon_0/\Lambda,\\ \Delta(1/m_\parallel)&=\alpha_\parallel T=-4B\epsilon_0/\Lambda,\end{aligned} \quad (26)$$

$T\|[111]$

$$\begin{aligned}\Delta(1/m_\perp')&=\alpha_\perp' T=\tfrac{2}{3}N\epsilon_0'/\Lambda,\\ \Delta(1/m_\parallel')&=\alpha_\parallel' T=-\tfrac{4}{3}N\epsilon_0'/\Lambda,\end{aligned} \quad (27)$$

where B and N are in units of $\hbar^2/2m_0$. (Here and in the rest of the paper unless otherwise stated the effective masses are given in units of the free electron mass m_0.) For $E_{3/2}$ all α's, of course, vanish. It is noticed that for the above uniaxial cases the shifts for $1/m_\parallel$ is opposite in sign to $1/m_\perp$ and twice the latter, i.e.,

$$\alpha_\parallel/\alpha_\perp=\alpha_\parallel'/\alpha_\perp'=-2.$$

For $T\|[110]$ both of the $J=\frac{3}{2}$ split-bands, in general, contain more or less an admixture of $M_J=\pm\frac{1}{2}$ and, consequently, both experience a mass shift. The three constants α_1, α_2, and α_3 for this case are given by Hasegawa.[22]

(2) *k^4-Mass Shift due to Incomplete Decoupling*

If the applied stress is insufficient to decouple the $E_{1/2}^+$ and $E_{3/2}$ states completely, then the nonparabolic nature of the energy bands near $\mathbf{k}=0$ becomes significant. Although the energy surfaces are nearly ellipsoidal, they exhibit some residual warping characteristic of the original energy surfaces. This perturbation is of second order in k^2 giving a k^4 mass shift. Under large stresses when ϵ_0 or $\epsilon_0'\gg k\Theta$, the bands are expected to

[22] Reference 10, Eq. (3.25).

be decoupled completely. However, even under these apparently ideal conditions, a small mass shift persists if extrinsic carrier heating mechanisms can upset the thermal equilibrium distribution and significantly populate the regions deep in the band (energies $\gtrsim \epsilon_0$ or ϵ_0') that are still warped. The correct interpretation of experimental results, therefore, requires that the k^4 perturbation be taken into account. Hasegawa[10] has shown that the k^4 shift for the inverse effective mass can be essentially lumped into a single term γ/T where γ is an anisotropic constant (which is negative in the present case for compressive stresses). The net effect of the term γ/T is always to *increase* the magnitude of the effective mass m^*. In addition, the line shift is accompanied by asymmetric line broadening showing a tail on the high-mass side. These asymmetries and the general question of line shapes are discussed in Sec. IV E.

In summary, the experimentally observed inverse effective mass is expected to vary as a function of stress T according to

$$\frac{1}{m^*}=\frac{1}{m_0^*}+\alpha T+\frac{\gamma}{T}, \tag{28}$$

where m_0^* is the zeroth order or unperturbed effective mass and α and γ are the linear and k^4-mass shift parameters, respectively. Equation (28) is used in Sec. IV C to fit empirically the stress dependence measured for the effective mass in order to obtain values for m_0^* and the correction terms involving α and γ.

III. EXPERIMENTAL DETAILS

The cyclotron resonance experiments were done on a balanced bridge cavity spectrometer operating at $\sim$8900 Mc/sec of the type[23] characteristic of spin resonance experiments. (The microwave frequency was monitored by a PRD 559B precision wave meter which was checked frequently with an HP 540A transfer oscillator in combination with an HP 524 frequency counter.) The rectangular cavity resonated in the TE_{101} mode. Superheterodyne detection made it possible to operate at the ultra-low power levels of 10^{-7} to 10^{-8} W necessary to prevent microwave heating of the carriers. Such heating is evidenced by broadening of all cyclotron resonance lines as well as *shifts* of the split-band hole lines This last point is discussed more fully later. Since the cyclotron resonance lines were observed to narrow significantly with decreasing temperature, all measurements were made at 1.26°K, the lowest temperature that could be conveniently reached. The dc magnetic field H_0 was measured by nuclear magnetic resonance The samples used were cut from a single crystal of Merck 5000 Ω cm p-type silicon. These crystals exhibited exceptionally long scattering relaxation times—at 1.26°K the electron lines had an $\omega\tau\sim160$.

After cutting, the samples were lightly etched for a few minutes in a solution made of 8 parts of HNO_3 and 1 part of HF. This reduces the surface recombination as well as eliminates sharp discontinuities which might lead to breakage under strain.

The samples were strained as follows: The rectangular shaped silicon samples were mounted 1 mm above the cavity floor opposite the coupling hole in a region well out of the maximum E field. The compressive uniaxial stresses were achieved by forces transmitted to the sample by external loading on the halves of the split cavity. A detailed description of the mechanical system used here, the "parallel squeezor," has been given elsewhere.[24] It should be noted that the squeezor makes possible exact control of the stresses by means of a calibrated spring balance located outside of the cryostat. In the geometry of the parallel squeezor the dc magnetic field H_0 could be rotated by angle φ in the plane of the stress T to measure the anisotropies of the effective masses. The E field is perpendicular to T so the cyclotron resonance absorption vanishes at $\varphi=90°$. In some instances the "perpendicular squeezor" was employed to permit rotation of H_0 azimuthally about the stress axis. Although stresses in silicon as high as 5000 kg/cm² have been reached by this method, it was done at the expense of sample cross section. Usually it was more desirable for the sake of strain uniformity and signal intensity to use larger samples, typically of dimensions 7 mm×3.5 mm×0.7 mm, and compromise with lower stresses $\sim$2500 kg/cm². Such samples, considerably shorter than the inside of the cavity, were accommodated by the use of quartz spacers between the ends of the sample and the cavity walls. Thin cardboard pieces cemented to the faces of the quartz pieces allowed the sample to "seat" itself and prevented localized strain concentration points. A small Teflon jig, in which the sample was free to move longitudinally, prevented lateral play during mounting and assembly of the apparatus.

The calibration of the squeezor was made, first, by calculation of the mechanical advantage of the mechanism and, second, by actual measurement of the compressive force from the elastic distortion of steel proving rings inserted between the squeezor jaws in place of the cavity. The two results agreed within a few percent. The stress, obtained from this calibration along with an accurate measurement of the sample cross section, was used to calculate the strains using the values for the elastic stiffness constants for silicon taken from the curves of McSkimin[25] extrapolated to 1.26°K: $c_{11}=17.09\times10^5$ kg/cm², $c_{12}=6.65\times10^5$ kg/cm², and $c_{44}=8.17\times10^5$ kg/cm². It was estimated that the stress or strain could be determined by this procedure to an over-all accuracy of about 5%.

Some evidence was found to suggest the presence of

[23] G. Feher, Bell System Tech. J. **26**, 449 (1957).

[24] D. K. Wilson and G. Feher, Phys. Rev. **124**, 1068 (1961).

[25] H. J. McSkimin, J. Appl. Phys. **24**, 988 (1953).

slight stress gradients in the sample. Such nonuniformities, if serious, could broaden the hole lines which are known to be shifted by strain. While no line broadening of this kind was noted, a $\frac{1}{2}\%$ shift expected from 5% variation of stress throughout the sample would not be observable because of the intrinsic linewidths of the resonances. On the other hand, small differences in the measured magnitude of the linear mass shifts were observed from run to run. This probably was due to a tendency of the sample to buckle slightly under load. Since the main contribution to the cyclotron resonance signal comes from the upper surface of the sample which is illuminated and also is in the strongest E field, the "observed" line shifts are most sensitive to the state of the strain in this region. These effects were minimized by averaging over a sequence of runs with the sample turned over between each.

Free carriers—both holes and electrons—were introduced into the sample by white light. The light, furnished by a 6-V microscope lamp (Spencer-type 353), was transmitted via a quartz light pipe running inside the waveguide down the Dewar and illuminated the sample through the cavity coupling hole. The linewidths of the cyclotron resonance signals, especially those for the electrons, were found to be very sensitive to excessive light intensity. The lines were narrowest when the light intensity was cut by operating the lamp "yellow" at 4 V and inserting into the beam a neutral density optical filter having 5% transmission Cyclotron resonance was also done with infrared illumination at a wavelength near that corresponding to the band gap of silicon. For these experiments a Bausch & Lomb 500-mm grating monochromator with the grating blazed for 1.0 μ was used. In all cases the cyclotron resonance absorption was modulated by chopping the light at 100 cps. The resulting signal was coherently detected.

Although the samples were oriented with an x-ray goniometer to within $\sim 0.3°$ of the desired crystallographic axis before cutting, special precautions were necessary to insure after mounting that the *stress* direction coincided with the crystal axis. For this purpose the electron lines in the cyclotron resonance spectrum were used as guide posts since their positions are essentially fixed as the stress is applied. From the positions of the electron lines the orientation of the crystal axis could be accurately determined. Likewise, the symmetry of the anisotropies of the masses of the strain-split hole line about T, was used to determine the direction of T. The two measurements located the stress axis relative to the crystal axis at the beginning of each run to within 0.2°. In all cases the maximum misorientation was kept less than 1.0°. For measurement with $T\|[001]$ or $T\|[110]$ where the effective masses are extrema a misorientation of this magnitude causes a negligible error of less than 1 part in 10^3.

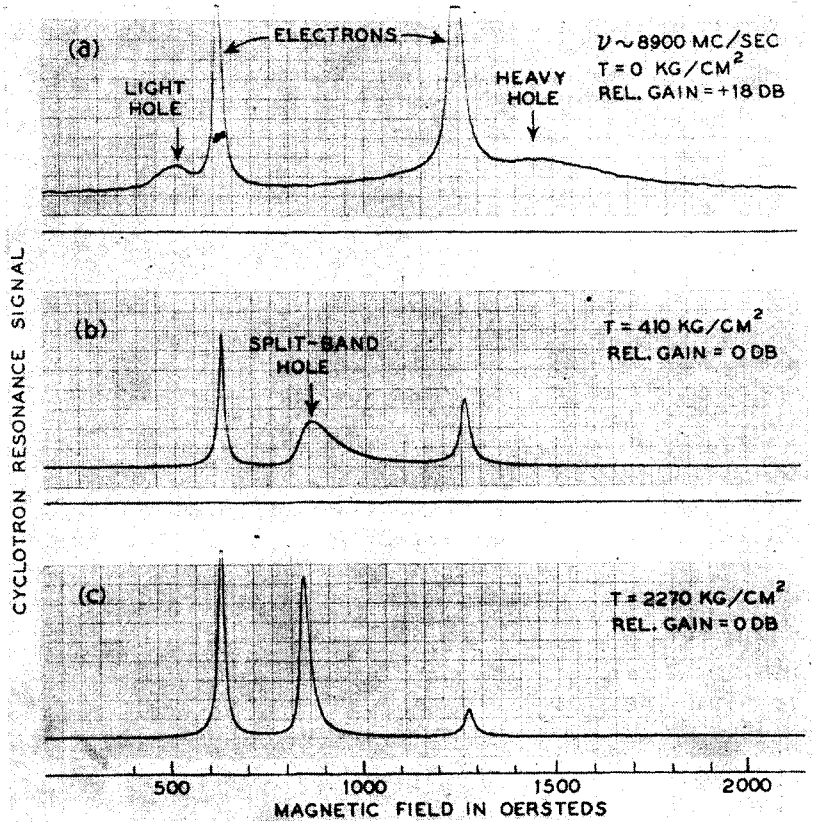

FIG. 3. The behavior of the cyclotron resonance lines in silicon as a uniaxial, compressive stress is applied along the [001] axis. The recorder traces were taken at 1.26°K and $\nu \approx 8900$ Mc/sec with H_0 in the (1$\bar{1}$0) plane and inclined 15° from the [001] axis. The broad, weak lines of the unstrained "classical" hole resonances in (a) point up the difficulties mentioned in Sec. II in obtaining accurate measurements of their effective masses.

For $T\|[111]$, however, the formulas given in Appendix C were used to correct for the *first-order* errors in mass arising from small misalignments of T. In all cases the corrections were less than $\frac{1}{2}\%$.

IV. EXPERIMENTAL RESULTS

A. General Features of the Spectrum

The application of a uniaxial stress to silicon causes marked changes of the hole lines in the cyclotron resonance spectrum as the initially degenerate valence band is split. The effects observed are illustrated in Fig. 3 showing typical recorder tracings of the cyclotron resonance lines with $H_0\|[111]$ taken for unstressed silicon as well as silicon subjected to a compressive, uniaxial stress along the [111] axis. As increasing stress is applied to the sample we find, first, for low stresses $T<100$ kg/cm^2 that the intensity of the light-hole line drops sharply as the descending band depopulates at liquid He temperatures. No mass shift is apparent for this line before it becomes too weak to be measured. The heavy hole, however, shifts to lower mass at the same time broadening to an extent such as to become unresolvable when T reaches $\sim$100 kg/cm^2. Next, when the stress exceeds $T\sim200$ kg/cm^2 the split-band hole line, very broad at first, begins to form in the intermediate mass region as shown in Fig. 3(b). As the bands decouple further, the hole line narrows rapidly and shifts to lower mass [the γ/T term in Eq. (28)] reaching a minimum mass value at $T\sim800$–1000 kg/cm^2. Finally, at this point the linear mass shift becomes evident [see Fig. 7(a)]. A small asymmetry in the line shape is noticeable even at the highest stresses reached ($T\sim2500$ kg/cm^2), indicating residual effects corrected with the k^4 mass shift.

A study of the line shape, k^4 mass shift, and related effects, which stem from a new line-broadening mechanism for cyclotron resonance, is used to check the theoretical basis for Eq. (28). These matters are taken up in Sec. IV E. It is important to note, however, that a detailed understanding of the line broadening is not essential for the application of Eq. (28) to the determination of the effective masses m_0^* in the discussions to follow.

B. Anisotropies of the Effective Masses

The anisotropies of the effective masses with respect to the angle φ between H_0 and T are shown in Figs. 4(a) and 4(b) for compressive stresses along the [001] and [111] directions, respectively. These anisotropies, characteristic of oblate elliposidal energy surfaces, indicate that $m_\perp>m_{\|}$ for $T\|[001]$ and $m_\perp'>m_{\|}'$ for $T\|[111]$. Since $T<0$, it follows according to Eq. (12) and (18) that

$$\begin{aligned} BD_u&<0,\\ ND_u'&<0. \end{aligned} \tag{29}$$

The effective masses measured in a plane perpendicular to T have been found to be isotropic for large stresses indicating essentially complete decoupling of the bands.

When $T\|[110]$ the energy ellipsoids have, in general, three unequal principal axes. This is illustrated by the effective mass anisotropies in Fig. 5 measured for H_0 in two, $(00\bar{1})$ and $(1\bar{1}0)$, of the three principal planes.

It is tempting to take values for the effective masses from Figs. 4(a) and 4(b). This procedure is incorrect, however, since we must analyze the behavior of m^* vs stress according to Eq. (28) to determine the zero-order mass m_0^*. This is done in the next section.

C. Dependence of the Effective Masses on the Stress

1. *Experimental Results*

The effective masses of the split-band hole in Si being functions of stress made it necessary to measure the dependence of m^* vs the stress T in order to determine the unperturbed masses m_0^* in addition to the parameter α. This procedure was facilitated by the external loading feature of the "squeezor" (see Sec. III) which allowed us to vary the stress on the sample form 0–2500 kg/cm^2 covering the range from the formation of the split-band hole at $T\sim400$ kg/cm^2 well into the linear region of the mass shift. Measurements were usually made at two angles, sufficient to define the anisotropy, by rotating the Varian magnet from $\varphi\sim0°$ for $H_0\|T$ to $\varphi\sim60°$–$70°$, the highest angles

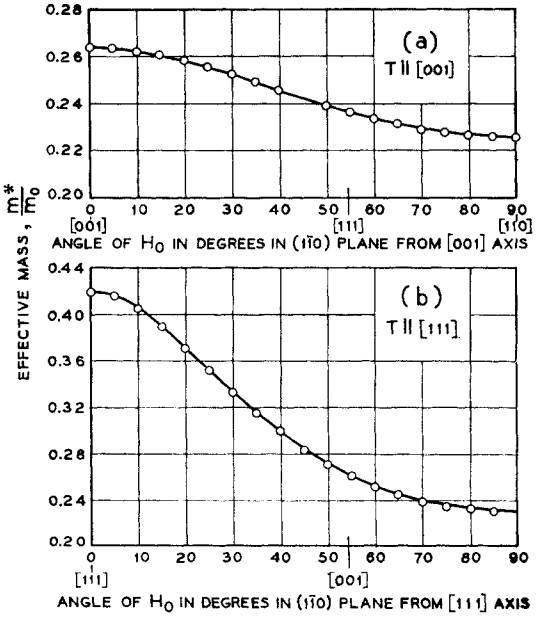

FIG. 4. The anisotropy of the "cyclotron" effective mass m^* for the hole resonance in uniaxially stressed silicon. For (a) $T=2130$ kg/cm^2 and (b) $T=1925$ kg/cm^2. The curves were calculated for ellipsoidal energy surfaces with (a) $m_\perp=0.2638$ and $m_{\|}=0.1929$ and (b) $m_\perp=0.4197$ and $m_{\|}=0.1255$.

that could be reached before the signal to noise for the cyclotron absorption became prohibitively poor for accurate measurements (see Sec. III).

The resulting measurements of m^* (taken at the maximum of the absorption line) were analyzed by fitting the experimental points, as shown by typical examples in Figs. 6–8, with curves calculated from Eq. (28). The excellent fit in all cases attests to the essential correctness of Eq. (28) in describing the stress dependence of the effective masses over the stress region 400–2500 kg/cm². From the values of $m_0^*(\varphi)$ for $T\|[001]$ and $T\|[111]$ thus obtained, the components $m_\perp$ and $m_\parallel$ of the effective mass tensor were calculated according to Eq. (D4) in Appendix *D*. Similarly the components $\alpha_\perp$ and $\alpha_\parallel$ of the linear mass shifts were derived from $\alpha(\varphi)$ by Eq. (D5) in Appendix D. An analogous procedure was used for $T\|[110]$ to get m_1, m_2, and m_3 [see Eq. (D7)]; and α_1, α_2, and α_3 [see Eqs. (D8) and (D10)].

The components of the effective mass tensors and the linear mass shift parameters α obtained in this way are given in Table II for T along [001], [111], and [110]. The results quoted represent averages from four to six different runs taken at each of the directions chosen for H_0. The uncertainties are based on the rms deviations from the average. It is believed that these represent the *experimental* uncertainties. However, any systematic error due to the lack of validity of Eq. (28) is not included. In our preliminary report on these measurements[11] no attempt was made to correct for the stress dependence of the masses. Consequently, the earlier values for $m_\perp$ were higher and those for $m_\parallel$ lower than the corrected ones quoted in this work.

As a by-product of these measurements we obtained (see captions of Figs. 6–8) representative values of γ, the k^4-shift contribution. The sign of this shift is always negative as predicted; and the magnitude appears to be highly anisotropic. Little quantiative significance can be attached to the magnitudes, however, because they varied as much as 40% from run to run depending upon conditions of illumination, changes in microwave power, etc. Under the same circumstances, the values for m^* and α were usually reproducible to better than 1 and 5%, respectively. This suggests that extrinsic carrier heating effects as well as the intrinsic k^4 shift were for the most part absorbed into the γ/T term.

2. *Determination of the Signs of D_u and D_u' from the Linear Mass Shifts*

From the existence of the linear shifts of the type characteristic of mixing of the $E_{1/2}^+$ and $E_{1/2}^-$ states of the valence bands, we conclude that the $E_{1/2}^+$ states lie above the $E_{3/2}$ states for silicon under compressive stress for both $T\|[001]$ and $T\|[111]$. Thus, the signs of the deformation potentials are fixed: $D_u>0$ and $D_u'>0$. This assignment is consistent with additional evidence available from the $T\|[110]$ measurements. Since the linear shift for $T\|[001]$ is small, it is especially

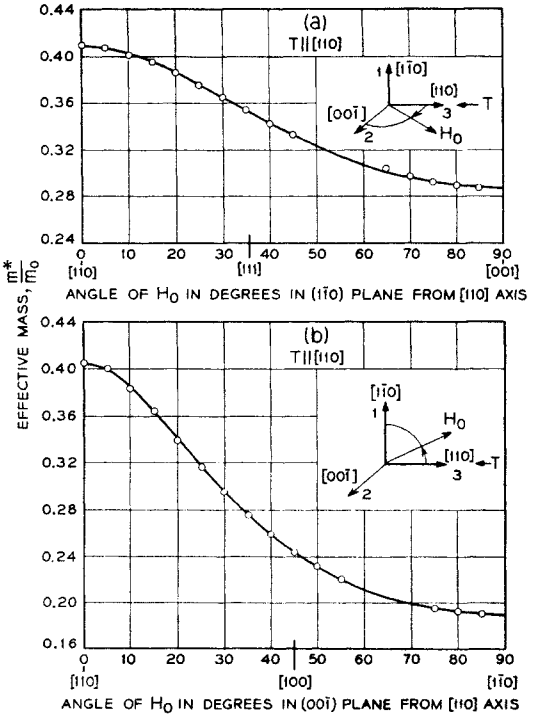

FIG. 5. The anisotropy of the effective mass m^* for the hole resonance in silicon with $T\|[110]$. For (a) $T=2270$ kg/cm² and (b) $T=2350$ kg/cm². The curves were calculated for ellipsoidal energy surfaces with (a) $(m_1m_2)^{1/2}=0.4085$ and $(m_1m_3)^{1/2}=0.2880$ and (b) $(m_1m_2)^{1/2}=0.4056$ and $(m_2m_3)^{1/2}=0.1905$.

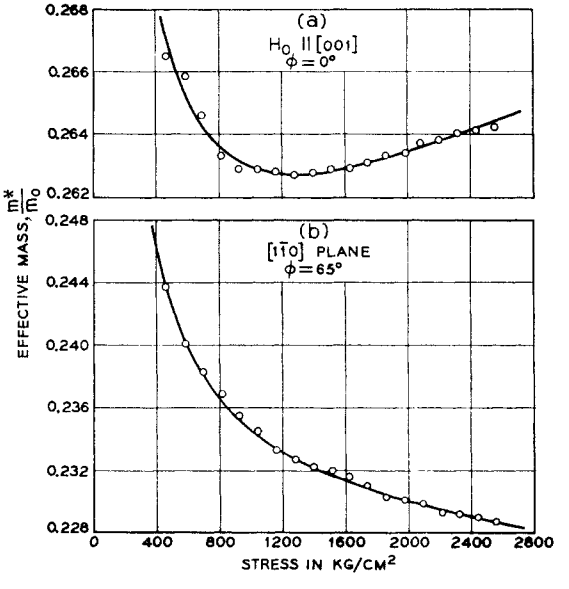

FIG. 6. The dependence of the effective mass m^* on stress for holes in uniaxially stressed silicon with $T\|[001]$. The curves were calculated for (a) $m_0^*=0.2557$, $\alpha=-0.40\times10^{-4}$ cm²/kg, and $\gamma=-68$ kg/cm²; and for (b) $m_0^*=0.2294$, $\alpha=+0.23\times10^{-4}$ cm²/kg, and $\gamma=-120$ kg/cm².

TABLE II. The components of the effective mass tensors (in units of the free electron mass m_0) and the linear mass shift parameters for silicon subjected to uniaxial, compressive stresses along the principal crystallographic directions [001], [111], and [110]. The experimental uncertainties indicated are based on the rms deviations from the averages of 4 to 6 runs.

$T\|\|[001]$	$T\|\|[111]$	$T\|\|[110]$
$m_\perp=0.2561\pm0.0010$	$m_\perp'=0.3695\pm0.0010$	$m_1=0.4390\pm0.0015$
$m_\parallel=0.1991\pm0.0015$	$m_\parallel'=0.1354\pm0.0010$	$m_2=0.2596\pm0.0015$
		$m_3=0.1486\pm0.0015$
$\alpha_\perp=-(0.40\pm0.05)\times10^{-4}$ cm²/kg	$\alpha_\perp'=-(1.55\pm0.10)\times10^{-4}$ cm²/kg	$\alpha_1=-(3.08\pm0.30)\times10^{-4}$ cm²/kg
$\alpha_\parallel=+(1.31\pm0.15)\times10^{-4}$ cm²/kg	$\alpha_\parallel'=+(3.22\pm0.20)\times10^{-4}$ cm²/kg	$\alpha_2=-(0.25\pm0.15)\times10^{-4}$ cm²/kg
		$\alpha_3=+(3.05\pm0.30)\times10^{-4}$ cm²/kg

important to check the sign assignment for D_u. Let us admit now for the sake of discussion the possibility that $D_u<0$ (and $B>0$). Using the values of the band parameters and deformation potentials in Table IV we can calculate[22] the values of α_1, α_2, and α_3 for the following two cases subject to the condition $BD_u<0$:

Case (i).

$$D_u>0, \quad B<0,$$
$$\alpha_1=-(2.31\pm0.25)\times10^{-4}\ \text{cm}^2/\text{kg},$$
$$\alpha_2=-(0.36\pm0.05)\times10^{-4}\ \text{cm}^2/\text{kg},$$
$$\alpha_3=+(2.67\pm0.25)\times10^{-4}\ \text{cm}^2/\text{kg}.$$

Case (ii).

$$D_u<0, \quad B>0,$$
$$\alpha_1=+(0.11\pm0.01)\times10^{-4}\ \text{cm}^2/\text{kg},$$
$$\alpha_2=+(0.08\pm0.01)\times10^{-4}\ \text{cm}^2/\text{kg},$$
$$\alpha_3=-(0.19\pm0.02)\times10^{-4}\ \text{cm}^2/\text{kg}.$$

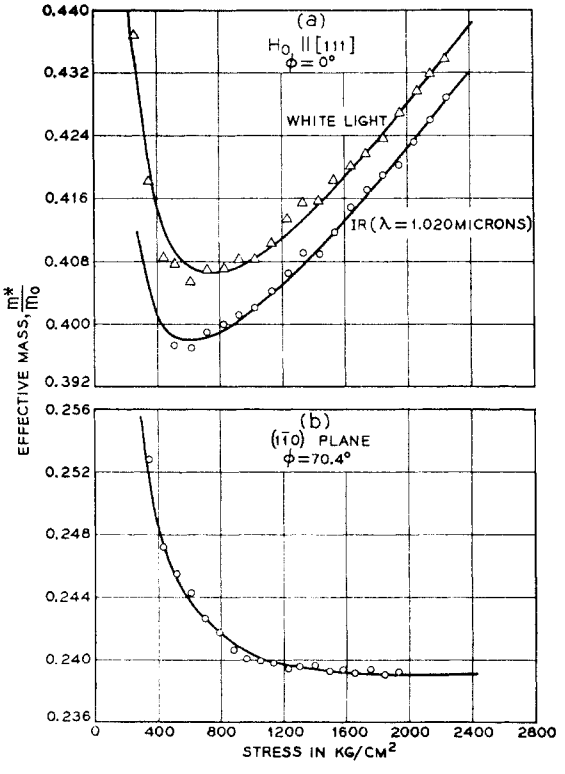

FIG. 7. The dependence of the effective mass m^* on stress for holes in uniaxially stressed silicon with $T\|[111]$. The curves were calculated for (a) (white light) $m_0^*=0.3704$, $\alpha=-1.60\times10^{-4}$ cm²/kg, and $\gamma=-90$ kg/cm² and (1.02 μ radiation) $m_0^*=0.3693$, $\alpha=-1.55\times10^{-4}$ cm²/kg, and $\gamma=-60$ kg/cm²; and for (b) $m_0^*=0.2335$, $\alpha=-0.25\times10^{-4}$ cm²/kg and $\gamma=-100$ kg/cm².

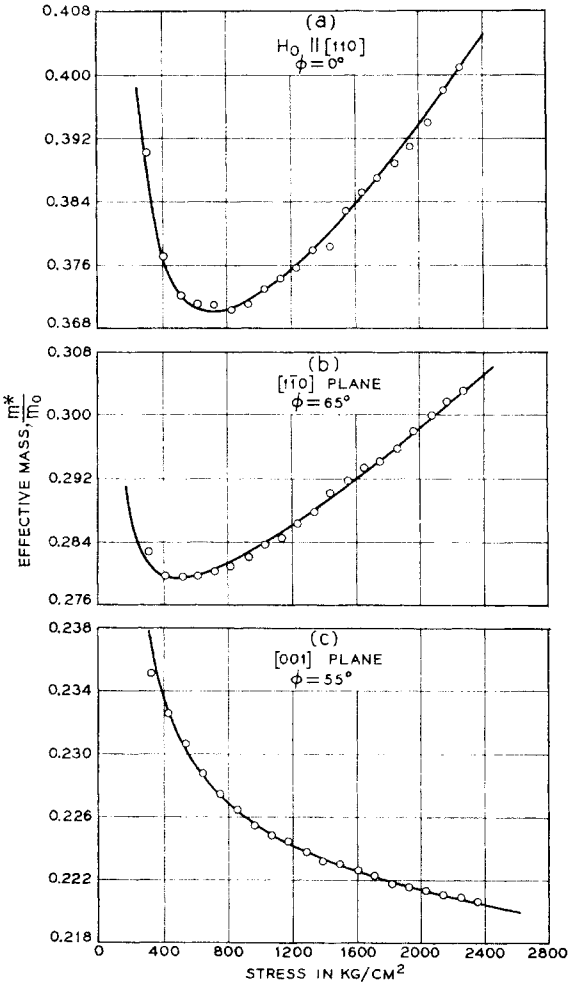

FIG. 8. The dependence of the effective mass m^* on stress for holes in uniaxially stressed silicon with $T\|[110]$. The curves were calculated for (a) $m_0^*=0.3350$, $\alpha=-2.00\times10^{-4}$ cm²/kg, and $\gamma=-100$ kg/cm²; (b) $m_0^*=0.2655$, $\alpha=-1.95\times10^{-4}$ cm²/kg, and $\gamma=-45$ kg/cm²; and (c) $m_0^*=0.225$, $\alpha=+0.35\times10^{-4}$ cm²/kg, and $\gamma=-90$ kg/cm².

Comparison of these numbers with the experimental results in Table II shows clearly that case (i) is the only possible choice.

3. *Other Possible Linear Mass Shifts*

The possibility exists that under strain the $J=\frac{3}{2}$ valence band can interact with other nearby bands (interband coupling), e.g., the Γ_2, conduction band, resulting in additional *linear* mass shifts besides that arising from the intraband mixing of the $E_{1/2}$ and $E_{1/2}^-$ states. To estimate the contribution from these sources, we use a theorem given by Hasegawa, namely,

$$\sum_{i=1,2,3} 1/m_i^*=3A \tag{30}$$

[where A, given by Eq. (4), here is in units of $\hbar^2/2m_0$] if the interband couplings can be neglected. Clearly, if the condition

$$\sum_{i=1,2,3} \alpha_i=0 \tag{31}$$

is obeyed, then it follows that the sum of inverse masses is invariant under stress as required in Eq. (30). Equation (31) is satisfied automatically if the α's arise only from *intraband* mixing since $\alpha_{11}/\alpha_\perp=\alpha_{11}'/\alpha_\perp'=-2$ as pointed out in Sec. II. The measured ratios

$$\begin{aligned}\alpha_{11}/\alpha_\perp&=-3.3\pm0.8,\\ \alpha_{11}'/\alpha_\perp'&=-2.01\pm0.10,\end{aligned} \tag{32}$$

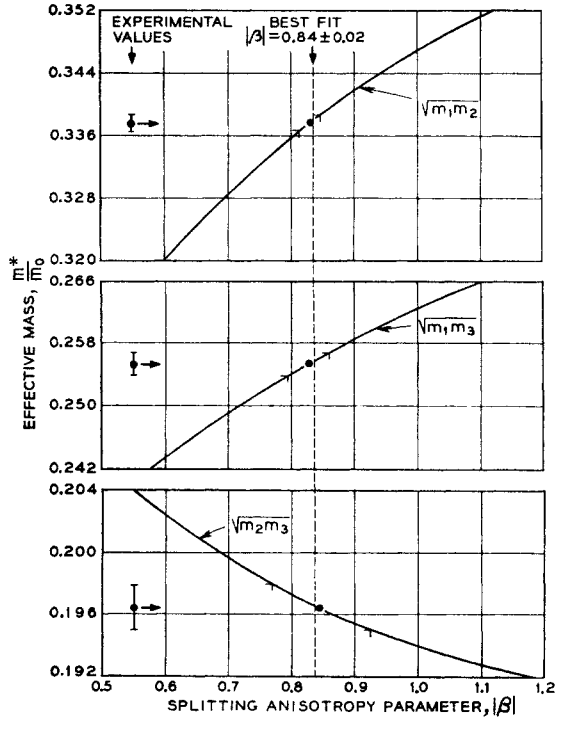

FIG. 9. Determination of the splitting anisotropy parameter β. [See Sec. II, Eq. (25).] The curves were calculated using the values of A, B, and N given in Table II.

are sufficiently close to the value -2 to allow us to conclude that interband mixing is probably unimportant, particularly so far $T\|[111]$. The larger discrepancy for the $T\|[001]$ case is not surprising in view of the small value of the shifts allowing, consequently, a greater relative contribution from other causes. For $T\|[110]$ we see that

$$\sum_{i=1,2,3} \alpha_i=0.3\pm0.3\sim0, \tag{33}$$

which is small in comparison to the intraband effects characterized by $\sum_{i=1,2,3}|\alpha_i|=6.4$, further supporting the contentions above.

D. The Determination of the Inverse Mass Band Parameter and the Deformation Potentials

From the effective masses in Table II the inverse mass band parameters are obtained at once by means of Eqs. (12) and (18). Since we have already ascertained that $BD_u<0$, $ND_u'<0$ and $D_u>0$, $D_u'>0$, it follows that B and N are both *negative*. The results for A, B, and N (in units of $\hbar^2/2m_0$) are summarized in Table III.

TABLE III. The inverse mass band parameters A, B, and N (in units of $\hbar^2/2m_0$); the deformation potentials D_u and D_u'; and the splitting anisotropy paramcter β for the valence bands of silicon. In calculating D_u and D_u' the value of the spin-orbit splitting was taken as $\Lambda=0.0441$ eV.[a]

$T\|[001]$	$T\|[111]$	$T\|[110]$
$A=-4.28\pm0.02$	$A=-4.27\pm0.02$	
$B=-0.75\pm0.04$	$N=-9.36\pm0.10$	
$D_u=+(2.04\pm0.20)$ eV	$D_u'=+(2.68\pm0.25)$ eV	$\beta=+0.84\pm0.02$

[a] See reference 17.

These values differ considerably from those ($A=-4.0\pm0.2$, $|B|=1.1\pm0.5$, $|N|=7.5\pm0.5$) obtained from the original cyclotron resonance experiments on the valence band of unstrained silicon. In view of the limitations, cited in Sec. II, that one faces in doing conventional cyclotron resonance on energy surfaces as badly warped as those in silicon, the poor agreement of the old results is, perhaps, not unexpected. *Note added in proof.* Values of the inverse mass band parameters for silicon recently obtained [J. J. Stickler, H. J. Zeiger, and G. S. Heller, Phys. Rev. **127**, 1077 (1962)] from the quantum spectra disagree in some cases from those quoted in Table III. The reasons for this discrepancy are at present not clear. Experiments by one of us (J. C. H.) are underway which, it is hoped, will shed more light on this question.

The splitting anisotropy parameter β defined in Sec. II, Eq. (25) was determined from measurements with $T\|[110]$ as follows: Using the values of A, B, and N obtained for $T\|[111]$ we can calculate the effective masses m_1, m_2, and m_3 for $T\|[110]$ as a function of the parameter $|\beta|$. The result is shown in Fig. 9 where we have plotted the calculated "mean

masses" $(m_1m_2)^{1/2}$, $(m_1m_3)^{1/2}$, and $(m_2m_3)^{1/2}$ which are the quantities directly measured. On the same figure we indicate the experimental points thereby fixing $|\beta| = 0.84 \pm 0.02$. Since $D_u > 0$ and $D_u' > 0$, the sign of β is *positive*. The ratio of the deformation potentials, therefore, is $D_u'/D_u = 1.31 \pm 0.03$.

The over-all consistency of the results can be judged by noting that we have essentially measured a total of 7 effective masses whereas only 4 quantities are being determined. The three redundant masses, therefore, serve as a check on the measurements. First, we see that the two values of A obtained when $T \| [001]$ and $T \| [111]$ are in excellent agreement. Second, Fig. 9 shows that all three measured masses for $T \| [110]$ are consistent with one value of $|\beta|$. Such agreement would be unlikely if the band parameters cited herein were appreciably in error.

The deformation potential D_u' is determined according to Eq. (27) from $\alpha_\perp'$ rather than α_{11}' the value of the latter being somewhat less certain. Thus, we get

$$D_u' = \alpha_\perp' \Big/ \left(\frac{2}{9}\frac{N}{\Lambda} s_{44}\right) = +(60.9 \pm 6.0)\Lambda, \qquad (34)$$

from which $D_u' = +(2.68 \pm 0.25)$ eV using the value[17] $\Lambda = (0.0441 \pm 0.0004)$ eV for the spin-orbit splitting. Next, from

$$\beta = \frac{D_u'(s_{44}/2)}{D_u(s_{11} - s_{12})} = +0.84 \pm 0.02, \qquad (35)$$

we get $D_u = +(2.04 \pm 0.20)$ eV. The value for D_u arrived at in this way is expected to be more reliable than that which could be gotten directly from $\alpha_\perp$ or α_{11}. It is, nevertheless, interesting as a check to compare these two results. To do this let us write the ratio β in terms of $\alpha_\perp$ and $\alpha_\perp'$ using Eqs. (26) and (27) which give

$$\beta = \frac{\alpha_\perp' B}{\alpha_\perp (N/3)} = +0.90 \pm 0.10. \qquad (36)$$

This result is entirely consistent with the more accurately known value $|\beta| = 0.84 \pm 0.02$ obtained directly from the measured effective masses. The values[26] for D_u, D_u', and β are listed in Table III.

E. Cyclotron Resonance Line Shape

1. *Experimentally Observed Linewidths, Asymmetries, and Shifts as Functions of Temperature, Direction of H_0, and Stress*

There are considerable experimental checks of Hasegawa's theory of line broadening. Foremost is the excellent fit of the stress dependence of the effective mass for all cases shown in Figs. 6–8. This, in fact, provides a verification of the aspects of the theory pertinent to the determination of the effective masses as given in Eq. (28). More detailed checks can be made using the following experimental results:

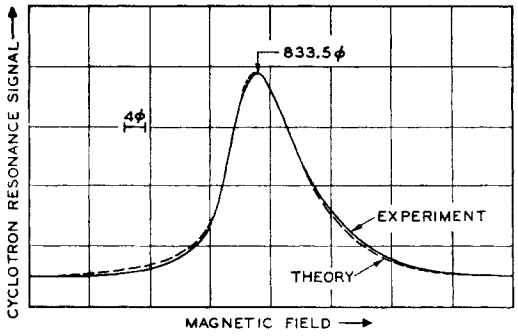

FIG. 10. Comparison of experimental and calculated line shapes of the hole resonance in silicon under uniaxial compressive stress. The experimental line shape was measured for H_0 and $T \| [001]$ ($T \cong 2550$ kg/cm^2), 1.35°K, and $\nu = 8816.4$ Mc/sec. The theoretical line shape was calculated by Hasegawa (reference 30) for 1.3°K, $\nu = 9000$ Mc/sec, and $|\omega_2|\tau = 0.4$. The width of the calculated line was matched to the measured resonance at the half amplitude points. The minor discrepancy between the curves is probably due partially to a small bridge unbalance in the spectrometer resulting in a slight admixture of the dispersive component into the absorption signal.

(a) For H_0 and $T \| [001]$ the k^4 contribution to the mass shift is measured to be $\gamma = 50$–70 kg/cm^2 at 1.3°K. The spread in these values appears largely due to carrier heating. It is expected, therefore, that the lower value in the range which was measured using infrared illumination of $\lambda = 1.02\,\mu$ is closest to the "intrinsic" value.

(b) A striking feature of the hole line in a sample subjected to a uniaxial stress is its asymmetry. This is clearly discernible in all the traces and is illustrated in detail in Fig. 10.

(c) The relative linewidth[27] varies inversely with stress as shown in Fig. 11 for H_0, $T \| [001]$ and 1.3°K. For $T = 2500$ kg/cm^2 the relative linewidth was measured to be $2\Delta H/H_0 = 1.5\%$.

(d) Under the conditions in (c) (T = 2500 kg/cm^2) the resonance line maximum exhibits a linear shift of $+1.1\%$ in raising the temperature from 1.3 to 4.2°K.

(e) The relative linewidth of the hole resonance is anisotropic with respect to the direction of H_0. This is shown in Fig. 12 for $T \| [001]$ and $T \| [111]$.

(f) The broadening of the lines with temperature is seen in Fig. 13. The exact dependence of the relative linewidth on temperature is plotted in Fig. 14 from which we see that $2\Delta H/H_0$ is proportional to the first power of the temperature Θ.

Before discussing the above results, it is interesting to note in passing that the electron lines (see Fig. 13)

[26] Calculations of the deformation potentials for silicon have recently been made by L. Kleinman (to be published). His results are $D_u = +2.85$ ev and $D_{u'} = +3.41$ eV.

[27] The linewidth $2\Delta H$ is defined as the total width at the half-amplitude absorption points.

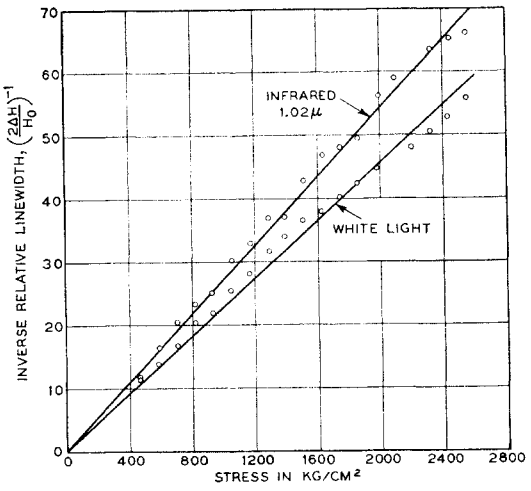

FIG. 11. Dependence of relative linewidth on stress for H_0, $T\|[001]$ (at 1.26°K and 8880 Mc/sec).

are completely symmetric, their linewidths arising from a relaxation time process. The ratio of scattering relaxation times for the electrons as measured from the linewidth $(2\Delta H/H_0=2/\omega_0\tau)$ is given by

$$\tau_e(1.26°\mathrm{K})/\tau_e(4.2°\mathrm{K})\simeq 6, \tag{37}$$

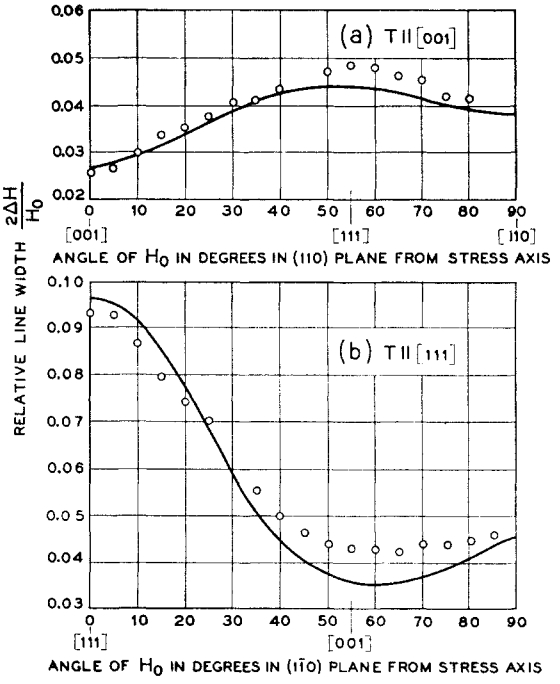

FIG. 12. Anisotropy of the relative linewidth of the hole resonance in uniaxially stressed silicon with respect to the direction of H_0 in the (1$\bar{1}$0) plane. The measurements were made at 1.26°K, $\nu\approx 8900$ Mc/sec, and for compressive stresses (a) $T=2130$ kg/cm² and (b) $T=1925$ kg/cm². The curves were calculated according to the theory of Hasegawa.

which fits very closely to a $\Theta^{-3/2}$ dependence,[28]

$$\frac{\tau(1.26°\mathrm{K})}{\tau(4.2°\mathrm{K})}=\left(\frac{1.26°\mathrm{K}}{4.2°\mathrm{K}}\right)^{-3/2}=6.1, \tag{38}$$

characteristic of acoustic phonon scattering.

The hole lines, on the other hand, exhibit an entirely different behavior suggesting the presence of a new line-broadening mechanism. First, the line shape is distinctly asymmetric with a tail on the high-mass side; second, the ratio of the linewidth changes only by a factor ~ 3 in going from 1.26 to 4.2°K. This is shown in more detail in Fig. 14.

2. *Comparison with Hasegawa's Line Broadening Theory*

These effects are explained by the line-broadening process proposed by Hasegawa.[10] Essentially each line is a superposition of a large number of individual lines corresponding to transitions between slightly unequally spaced Landau levels—a consequence of the nonparabolic nature of the split valence band (see Sec. II C) due to incomplete decoupling by strain. This "inhomogeneous broadening" differs from k_z broadening since the individual component lines of the former could be separated under sufficiently high resolution.[29] The frequency of the component line arising from a transition between the Landau levels $n\rightarrow n+1$ is given by

$$\omega_{n,k}=\omega_0+\omega_1+\omega_2 n+\omega_3 k^2. \tag{39}$$

Here ω_0 is the unperturbed (angular) frequency; ω_1 represents a "quantum" shift (which is the same for

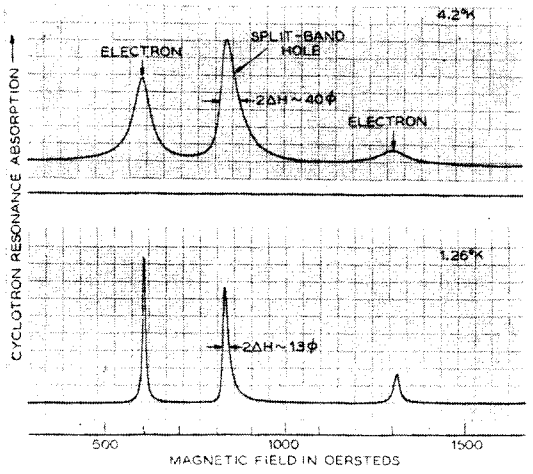

FIG. 13. Comparison of cyclotron resonance lines in uniaxially stresses silicon at 1.26 and 4.2°K. The traces were taken for H_0 and $T\|[001]$ ($T=2550$ kg/cm²) and $\nu\approx 8800$ Mc/sec.

[28] The $\Theta^{-3/2}$ dependence of the scattering relaxation time is confirmed in detail by measurements throughout the range 1.26 and 4.2°K, J. C. Hensel (unpublished). For measurements at higher temperatures, see D. M. S. Bagguley, R. A. Stradling, and J. S. S. Whiting, Proc. Roy. Soc. (London) **A262**, 365 (1961).

[29] The inhomogeneous broadening enables one, in principle, to saturate part of the hole resonance line and perform double resonance experiments analogous to ENDOR.

all component lines); ω_2 gives the spacing between component lines; and the ω_3 term includes k_z broadening which for the present case is negligible. The perturbation terms, ω_1, ω_2, and ω_3, are all inversely proportional to the stress T.

Raising the temperature increases the line broadening by shifting the hole population to the upper Landau levels. The lattice scattering dependence on temperature contributes only in a secondary way by broadening the component lines. For present conditions where the values of $\omega_0\tau$ appear to be large, the linewidth seems to be more or less dominated by the inhomogeneous or "k^4 broadening."

Hasegawa[30] has calculated representative line shapes by taking weighted sums of Lorentzian lines up to $n=20$, where n is the Landau quantum number, for the case T and H_0 along [001], $\omega_0=2\pi\times9000$ Mc/sec, and $\Theta=1.3$°K consistent with the experimental conditions for Figs. 10 and 11. These line shapes are characterized by the parameter $|\omega_2|\tau$ which gives the spacing, ω_2, between the component lines of the resonance relative to their half-width, $1/\tau$. From these calculated lines plotted against $x=(\omega-|\omega_0+\omega_1|)\tau$, the resonance maximum, $x_{\max}$ (which gives the shift of the composite line due to the ω_2 term) and the linewidth, Δx, have been determined and are given in Table IV.

At this point we cannot directly compare the linewidth Δx given in Table IV with the experimental linewidth $2\Delta H$ of the hole resonance because the former depends upon the as yet undetermined parameter $|\omega_2|\tau$ ($|\omega_2|$ and τ, in fact, are both unknown). Some light can be shed on this problem by the following approach.

Hasegawa[31] has determined an approximate expression for the linewidth from the second moment by assuming the component lines to be narrow compared to the resonance width but not narrow compared to the spacing between the component lines, i.e., $|\omega_2|\tau\sim1$ (it will be seen presently that $|\omega_2|\tau\sim0.4$ for the case at hand). Approximating the composite line by a Gaussian shape (thereby neglecting asymmetry), he has obtained the second moment value of the linewidth as

$$\frac{2\Delta H}{H_0}\approx 2.35\left|\frac{\omega_2}{\omega_0}\right|\sqrt{2\frac{k\Theta}{\hbar\omega_0}}. \tag{40}$$

Using Eq. (40) the measured relative linewidth $2\Delta H/H_0=1.5\%$ at 1.3°K gives $|\omega_2/\omega_0|\sim1.4\times10^{-3}$ for H_0, $T\|[001]$ and $T=2500$ kg/cm^2.

It is seen that Eq. (40) predicts a linear dependence of the linewidth on temperature consistent with the experimental results shown in Fig. 14. The observed linear dependence with temperature is evidence that one is not near the limiting case $|\omega_2|\tau\ll1$. If this were the case here, the linewidth of the resonance would be strongly influenced by the component linewidth and would, therefore, be expected to vary with temperature somewhat more like $\Theta^{3/2}$ as observed for the electron linewidths. Inasmuch as $|\omega_2/\omega_0|$ varies inversely with stress, Eq. (40) also predicts the observed inverse stress dependence of the relative linewidth as shown in Fig. 11.

Next, from the result $|\omega_2/\omega_0|\sim1.4\times10^{-3}$ just obtained we calculate $\omega_0\tau\equiv|\omega_2|\tau|\omega_0/\omega_2|$, the values of which are given in the fourth column of Table IV. These determine the relative linewidth $2\Delta H/H_0=\Delta x/\omega_0\tau$, the values for which are listed in the last column of Table IV. From the latter we find that the observed relative linewidth of 1.5% for 1.3°K and H_0, $T\|[001]$ coincides with the linewidth calculated for $|\omega_2|\tau=0.4$ and $\omega_0\tau\sim280$. This result has been checked by fitting the experimental line shape with the one calculated for $|\omega_2|\tau=0.4$. In Fig. 10 one sees that the agreement is quite satisfactory.

The hole resonance exhibits a relative line shift from $x=0$, i.e., $\omega=\omega_0+\omega_1$, by an amount $x_{\max}\omega_0\tau$. Thus, the

TABLE IV. Position of resonance maximum and linewidth for $\Theta=1.3$°K, $\omega_0=2\pi\times9000$ Mc/sec. The line is plotted against $x=(\omega-|\omega_0+\omega_1|)\tau$. The values for $\omega_0\tau$ and the relative linewidths $2\Delta H/H_0$ were calculated assuming $|\omega_2/\omega_0|=1.4\times10^{-3}$.

	Line maximum	Linewidth		
$\|\omega_2\|\tau$	$x_{\max}$	Δx	$\omega_0\tau$	$2\Delta H/H_0$
0.1	+0.48	2.33	71	3.3%
0.2	+0.86	2.92	143	2.0%
0.3	+1.17	3.54	214	1.7%
0.4	+1.46	4.18	286	1.5%
0.6	+2.03	5.54	430	1.3%
0.8	+2.51	6.79	570	1.2%

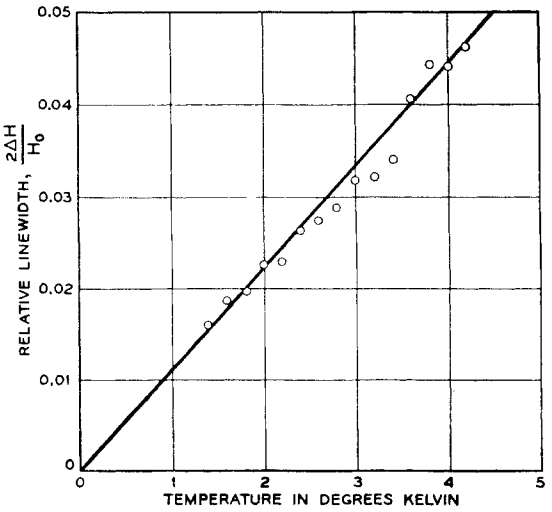

FIG. 14. Relative linewidth of the hole resonance in uniaxially stressed silicon vs temperature. The measurements were made for H_0 and $T\|[001]$ ($T=2550$ kg/cm^2) and $\nu\simeq8800$ Mc/sec.

[30] H. Hasegawa, reference 10 and (private communication). We are indebted to Dr. Hasegawa for supplying us with his unpublished calculations of line shapes.

[31] H. Hasegawa (private communication). See reference 10, Eq. (4.21).

total relative line shift from $\omega=\omega_0$ is given by

$$\frac{\Delta\omega}{\omega_0}=-\left(\left|\frac{\omega_1}{\omega_0}\right|+\frac{x_{\max}}{|\omega_2|\tau}\left|\frac{\omega_2}{\omega_0}\right|\right). \tag{41}$$

From this it follows that the term γ/T in Eq. (28) is

$$\frac{\gamma}{T}=-\frac{1}{m_0^*}\left(\left|\frac{\omega_1}{\omega_0}\right|+\frac{x_{\max}}{|\omega_2|\tau}\left|\frac{\omega_2}{\omega_0}\right|\right), \tag{42}$$

where γ, it should be noted, is independent of the applied stress T since both ω_1/ω_0 and ω_2/ω_0 are inversely proportional to T. A value for ω_1/ω_0 has not been ascertained experimentally. However, theoretical estimates made by Hasegawa[10] indicate that ω_1/ω_0 and ω_2/ω_0 are nearly of the same magnitude; the latter, therefore, having a sizable coefficient of $x_{\max}/|\omega_2|\tau \sim 3.6$ gives the major shift. Thus,

$$\gamma\sim-\frac{T}{m_\perp}\frac{x_{\max}}{|\omega_2|\tau}\left|\frac{\omega_2}{\omega_0}\right|\sim-50\ \text{kg/cm}^2 \tag{43}$$

for H_0, $T\|[001]$ and 1.3°K in good agreement with the experimental vaues $\gamma\sim-50$ to -70 kg/cm^2.

When the temperature is raised from 1.3 to 4.2°K, the resonance maximum H_0, $T\|[001]$ is observed to shift linearly by $+1.1\%$. It is difficult to see the temperature dependence from Eq. (41) as it stands although it is implicit in the coefficient $x_{\max}/|\omega_2|\tau$. However, if it is assumed that $|\omega_2|\tau\ll1$ (which is not strictly true here), Hasegawa[32] finds that the relative line shift is given by

$$\frac{\Delta\omega}{\omega_0}=-\frac{\omega_1}{\omega_0}+\frac{2k\Theta}{\hbar\omega_0}\left(\frac{\omega_2}{\omega_0}\right), \tag{44}$$

which explicitly contains the temperature Θ. In comparing the results at 1.3 and 4.2°K it is the last term that interests us. Thus,

$$\frac{\Delta m^*}{m^*}=-\frac{\Delta\omega}{\omega_0}=\frac{2k\Delta\Theta}{\hbar\omega_0}\left|\frac{\omega_2}{\omega_0}\right|, \tag{45}$$

giving a relative line shift of $\Delta m^*/m^*\sim+2\%$ for $|\omega_2/\omega_0|\sim1.4\times10^{-3}$. As pointed out by Hasegawa, Eqs. (44) and (45) overestimate the shift when $|\omega_2|\tau$ is not $\ll1$ the correction (see Table III, reference 10) being ~2 for $|\omega_2|\tau=0.4$. The relative linewidth is, accordingly,

$$(\Delta m^*/m^*)\ \text{(corrected)}\sim\tfrac{1}{2}\times2\%\sim+1\%,$$

in agreement with the measured value.

The relative linewidth of the hole resonance is anisotropic with respect to the angle φ between H_0 and T as illustrated in Fig. 12 for $T\|[001]$ and $T\|[111]$. Hasegawa[31] has obtained expressions for the anisotropies of $|\omega_2/\omega_0|$ for H_0 in the $(1\bar{1}0)$ plane and for $T\|[001]$ and for $T\|[111]$. Under conditions which Eq. (40) holds, it follows that this also gives the anisotropy of the relative linewidth. The calculated results are shown in Fig. 12. There is a qualitative fit for both cases $T\|[001]$ and $T\|[111]$. Finally, from the measurements shown in Fig. 12 it is possible to compare $2\Delta H/H_0$ for the two cases H_0, $T\|[001]$ and H_0, $T\|[111]$. The calculated ratio[33] for $H_0\|T$ is

$$\left|\frac{\omega_2[111]}{\omega_2[001]}\right|=\left|\frac{\epsilon_0}{\epsilon_0'}\right|\frac{2}{3}\left(\frac{m_\perp'}{m_\perp}\right)\frac{[B^2+2(N/3)^2]}{[B^2+(N/3)^2]}=3.6, \tag{46}$$

which is very close to the measured ratio of 3.7.

As mentioned earlier the parameter $|\omega_2/\omega_0|$ can be estimated theoretically. Using the experimental values of $m_\perp/m_0$, B, N, and D_u given in Sec. IV D, it is found for H_0, $T\|[001]$ and $T=2500$ kg/cm^2 that $|\omega_2/\omega_0|\sim2.8\times10^{-3}$ which is twice the value determined experimentally. This discrepancy is not understood.

We conclude that the generally good agreement in the foregoing examples between the predicted and observed behavior of the line shapes substantiates in some detail the Hasegawa line-broadening theory.

3. *Line Shifts due to Carrier Heating*

Thus far, we have assumed that the carriers are in thermal equilibrium with the lattice, and the Landau levels are populated according to an equilibrium Boltzmann distribution. Actually it has been found that a number of experimental factors can seriously upset this idealization.

First, excessive microwave power, especially if scattering relaxation times are long, can pump the carriers into the higher Landau levels thereby broadening and shifting the line. These effects are illustrated in Figs. 15 and 16 showing the line position for H_0 and $T\|[111]$ as a function of microwave power, P_0, coupled to the cavity. Under extreme conditions, $P_0\sim10^{-2}$ W, the split-band hole resonance can be shifted nearly to the position of the original heavy hole.

Second, "hot" carriers can be produced by the illuminating radiation if $h\nu>E_{gap}$ as indicated in Fig. 7(a). The effective mass for $T\|[111]$ is shown for white light and monochromatic radiation of wavelength 1.02 μ close to the band gap. A distinct line shift is evident especially for low values of stress. Although less pronounced than the microwave effects, this light shift, nevertheless, can cause sizable errors in effective mass measurements. Fortunately, its effects can for the most part be extracted from the data using the mass shift analysis given in Eq. (28). These heating effects shift the values for γ but have little effect on the values of m_0^* and α. (See caption of Fig. 7.) It is, however,

[32] Reference 10, Eq. (4.19).

[33] See Eq. (4.16) and (4.24) of reference 10.

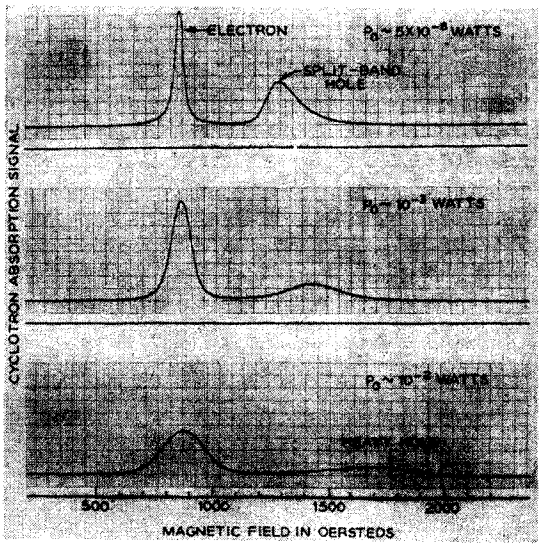

FIG. 15. The effects of microwave carrier heating upon the cyclotron resonance lines in uniaxially stressed silicon. The traces were taken for H_0 and $T\|[111]$ ($T\approx1000$ kg/cm^2), 1.26°K, and $\nu\approx8900$ Mc/sec. In (c) the high microwave electric fields ($E_1\approx10$ V/cm) shift the split-band hole line nearly to the position indicated for the unstressed "heavy" hole line. The electron lines are severely broadened by the microwave carrier heating at the power levels 10^{-3} to 10^{-2} W in (b) and (c).

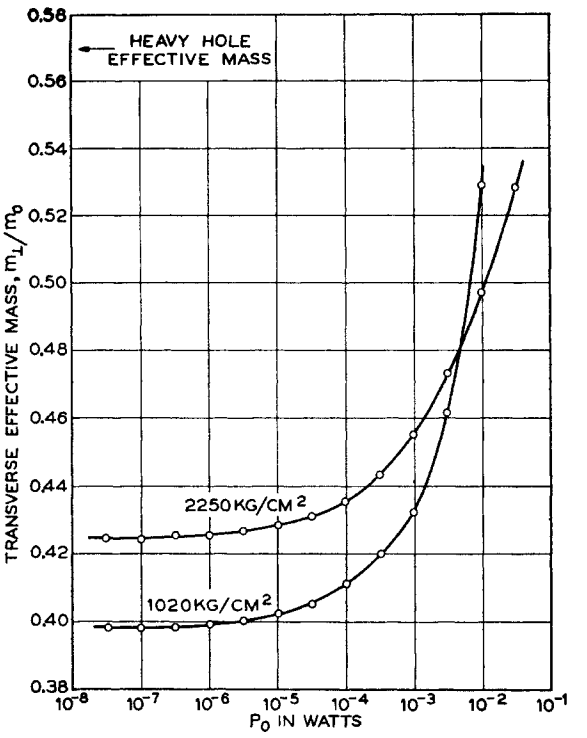

FIG. 16. The effective-mass shifts of the hole resonance produced by microwave carrier heating. The data were taken for H_0 and $T\|[111]$, 1.26°K, and $\nu\approx8900$ Mc/sec. At $P_0=10^{-2}$ W the electric field in the sample was $E_1\approx10$ V/cm. For low power levels the curves fail to coincide because of the shift of effective mass with stress.

desirable to eliminate *all* heating mechanisms as much as possible from the experiments.

V. DISCUSSION

A. Negative Sign of B

Contrary to earlier theoretical predictions,[5] the sign of the band parameter B has turned out to be negative. This has important implications for the ordering of the conduction energy bands at the point $\Gamma(\mathbf{k}=0)$ as seen by the following argument: In essence, F, G, H_1, and H_2 each have the form

$$\frac{|\langle\Gamma_i|\,\mathbf{p}\,|\Gamma_{25'}\rangle|^2}{E_0-E_i},$$

where E_0 and E_i are, respectively, the energies of the valence band $\Delta_{25'}$ and the perturbing conduction band Γ_i according to the classification in Table I. Since the perturbing bands lie above $\Gamma_{25'}$ we expect that F, G, H_1, and H_2 are all negative. On the other hand, B can, in general, have either sign. From Eqs. (2) and (4), we see that $B=\frac{1}{3}(L-M)\sim\frac{1}{3}(F-H_1)$ if we ignore for the moment the contributions of G and H_2 which are small. Thus, the sign of B is, to a large extent, controlled by the relative magnitudes of F and H_1 which, in turn, depend upon the relative locations of Γ_2, and Γ_{15}, respectively. Hence, the negative sign measured for B implies that $\Gamma_{2'}$ is lower and Γ_{15} is higher than the earlier estimated positions making the band ordering in silicon more nearly like that in germanium.

Taking the measured values of A, B, and N from Table III we calculate F, G, and H_1 (in units of $\hbar^2/2m_0$):

$$\begin{aligned} F&=\tfrac{1}{3}(-A+4B+2N+1)=-5.48\pm0.06,\\ G&=\tfrac{1}{3}(2A+B-N-2)=-0.64\pm0.03,\\ H_1&=A-B-1=-4.51\pm0.05. \end{aligned} \tag{47}$$

As usual, the assumption has been made that $H_2\sim0$, justified since Γ_{25} is remote (~30 eV) from the valence band and since the matrix element itself is very small. Using the earlier values for the matrix elements (which are substantially less sensitive to the values of F, G, and H_1 than are the energies), Phillips[16] has recalculated the band energies using the new values of the band parameters in Eq. (47). He finds that $\Gamma_{2'}$ and Γ_{15} both fall at approximately 2.8 eV thus forming the direct energy gap at $\mathbf{k}=0$, and that $\Gamma_{12'}$ will fall somewhat higher at ~10 eV, approximately at its previous estimated position. Previously, $\Gamma_{2'}$ and Γ_{15} were believed to be at 8.8 and 2.1 eV, respectively. The revised estimate for the position of $\Gamma_{2'}$ is corroborated by recent evidence obtained by Tauc and Abraham[15] from the optical absorption in Ge–Si alloys which upon extrapolation to the limit of pure Si indicated that $\Gamma_{2'}$ is near 3.3 eV.

As mentioned earlier, the sign measured for B is in

contradiction to that obtained from band calculations.[5] The reason for the failure of the band calculations has been examined by Phillips.[16] He concludes that the difficulty lies in estimating reliably the value for the core levels relative to valence levels. Certain bands (at Γ, for instance, $\Gamma_{2'}$) are very sensitive to core level shifts as recently pointed out by Herman[34]; and it seems risky, therefore, to make detailed predictions without calculating core levels as carefully as valence levels. For silicon, the ordering of bands at Γ indicated by the cyclotron resonance data requires a value of core shift which is encouragingly close to that needed[16] to fit the peaks for optical absorption at $L(\mathbf{k}=(\pi/a)[111])$ measured by Tauc and Abraham.

B. Nearly Isotropic Band Splitting in Silicon

A further unexpected result of the present work has been that the $J=\frac{3}{2}$ band energy splitting is nearly equal for $T\|[001]$ and $T\|[111]$, and, furthermore, has the same sign, i.e., the order of states at $\mathbf{k}=0$ is the same for $T\|[001]$ and $T\|[111]$ with $M_J=\pm\frac{1}{2}$ "up" for compressive stress. As pointed out earlier, under these conditions, the energy splitting is isotropic with respect to the directions of T, and $\pm M_J$ is always a "good" quantum number along the direction of T. A similar result has been found recently for the valence band of CdTe by Thomas[35] from optical reflection measurements of the direct exciton in uniaxially stressed crystals. It is important to note that more nearly equal splittings are obtained for equal applied stress rather than strain. This implies a relationship between the deformation potentials and the elastic constants,

$$D_u(s_{11}-s_{12})\simeq D_u' s_{44}/2. \tag{48}$$

(Neither Si nor CdTe is elastically isotropic, i.e., for both $s_{11}-s_{12}\neq s_{44}/2$.) At present, there is no theoretical reason to expect such a property which may be purely "accidental" for Si and CdTe. It would be of interest to ascertain if a similar behavior exists in other cubic, tetrahedrally coordinated semiconductors.[36]

ACKNOWLEDGMENTS

It is a pleasure to thank J. J. Hopfield, E. O. Kane, W. Kohn, J. C. Phillips, and Y. Yafet for numerous discussions on subjects pertaining to these experiments. We are especially grateful to H. Hasegawa who communicated his results to us before publication and contributed many invaluable suggestions and comments during the course of this work. We would like to thank D. H. Sweet for his assistance in making the measurements.

[34] F. Herman and J. Skillman, *Proceedings of the International Conference on Semiconductor Physics, Prague, 1960* (Czechoslovakian Academy of Sciences, Prague, 1961), p. 20.
[35] D. G. Thomas, J. Appl. Phys. **32**, 2298 (1961).
[36] For germanium $\beta\sim 0.9\pm 0.2$ according to the values of the deformation potentials measured recently by J. J. Hall, Phys. Rev. **128**, 68 (1962).

VII. APPENDIXES

A. Strain Components for a Cubic Lattice

We calculate the strain components in a cubic crystal with an applied uniaxial stress along a direction in the $(1\bar{1}0)$ plane. This covers the cases for stress along each of the three principal crystallographic directions (a generalization to include cases when T is out of a $(1\bar{1}0)$ plane is easily made). The procedure is quite straightforward; but due to considerable confusion over a factor of 2 in some of the strain components it seems worthwhile to write out the analysis in detail.

Consider a Cartesian coordinate system (x',y',z') such that T' is along the z' axis. (The specific choice for x' and y' is unimportant.) In this system the stress tensor has the simple form

$$\|T'\|=\begin{vmatrix}0\\0\\T\\0\\0\\0\end{vmatrix} \tag{A1}$$

in 6-vector notation. In order to transform this tensor from the primed system into the crystal coordinate system (x,y,z) we need the coordinate transformation

$$x_i=(a^{-1})_{ij}x_j'. \tag{A2}$$

A simple choice for the x' and y' directions gives the transformation matrix

$$\|\alpha^{-1}\|=\begin{pmatrix}\frac{1}{\sqrt{2}} & \frac{1}{\sqrt{2}}\cos\theta & \frac{1}{\sqrt{2}}\sin\theta\\ -\frac{1}{\sqrt{2}} & \frac{1}{\sqrt{2}}\cos\theta & \frac{1}{\sqrt{2}}\sin\theta\\ 0 & -\sin\theta & \cos\theta\end{pmatrix}, \tag{A3}$$

where θ equals the polar angle between z and z'. The stress tensor rotates by the same transformation according to

$$T_{ik}=(\alpha^{-1})_{ij}(\alpha^{-1})_{kl}T_{jl}', \tag{A4}$$

so that in the crystal system (x,y,z) it becomes

$$\|T\|=\begin{vmatrix}T_{xx}\\T_{yy}\\T_{zz}\\T_{xy}\\T_{xz}\\T_{yz}\end{vmatrix}=T\begin{vmatrix}\frac{1}{2}\sin^2\theta\\\frac{1}{2}\sin^2\theta\\\cos^2\theta\\\frac{1}{2}\sin^2\theta\\(1/\sqrt{2})\sin\theta\cos\theta\\(1/\sqrt{2})\sin\theta\cos\theta\end{vmatrix}. \tag{A5}$$

Next, from the stress tensor (A5) we obtain the strain tensor by the relation

$$S_{ij}=s_{ijkl}T_{kl}, \tag{A6}$$

where the s_{ijkl} are components of the cubic elastic

compliance tensor[37]

$$\|s\|=\begin{Bmatrix} s_{11} & s_{12} & s_{12} & & & \\ s_{12} & s_{11} & s_{12} & & 0 & \\ s_{12} & s_{12} & s_{11} & & & \\ & & & \frac{1}{4}s_{44} & 0 & 0 \\ & 0 & & 0 & \frac{1}{4}s_{44} & 0 \\ & & & 0 & 0 & \frac{1}{4}s_{44} \end{Bmatrix} \tag{A7}$$

The strain tensor (written as a 6-vector) is, finally,

$$\|S\|=T\begin{Bmatrix} \frac{1}{2}s_{11}\sin^2\theta+s_{12}(\frac{1}{2}\sin^2\theta+\cos^2\theta) \\ \frac{1}{2}s_{11}\sin^2\theta+s_{12}(\frac{1}{2}\sin^2\theta+\cos^2\theta) \\ s_{11}\cos^2\theta+s_{12}\sin^2\theta \\ \frac{1}{4}s_{44}\sin^2\theta \\ (1/2\sqrt{2})s_{44}\cos\theta\sin\theta \\ (1/2\sqrt{2})s_{44}\cos\theta\sin\theta \end{Bmatrix} \tag{A8}$$

As usually defined, however, the "conventional" strain components e_{ij} differ from those of the tensor $\|S\|$ by a factor of 2 in the off-diagonal elements:

$$\begin{aligned} e_{xx}&=e_{yy}=T[\tfrac{1}{2}s_{11}\sin^2\theta+s_{12}(\tfrac{1}{2}\sin^2\theta+\cos^2\theta)] \\ e_{zz}&=T[s_{11}\cos^2\theta+s_{12}\sin^2\theta] \\ e_{xy}&=(T/2)s_{44}\sin^2\theta \\ e_{xz}&=e_{yz}=(T/\sqrt{2})s_{44}\cos\theta\sin\theta. \end{aligned} \tag{A9}$$

B. Effective Masses for a Uniaxial Stress in the $(1\bar{1}0)$ Plane

1. *Calculation of the Masses*

We consider now the general problem of calculating the principal masses m_1, m_2, and m_3 for the $J=\frac{3}{2}$ bands for an arbitrary orientation of T in the $(1\bar{1}0)$ plane. We start by writing the splitting part of the strain Hamiltonian from Eq. (16) using the strain components in (A9),

$$\begin{aligned} H_e=\epsilon(J_z^2-\tfrac{1}{3}J^2)+\tfrac{2}{3}\epsilon'\{J_xJ_y\} \\ +\tfrac{2}{3}\epsilon''(\{J_xJ_z\}+\{J_yJ_z\}), \end{aligned} \tag{B1}$$

where

$$\begin{aligned} \epsilon&=\epsilon_0(\cos^2\theta-\tfrac{1}{2}\sin^2\theta) \\ \epsilon'&=\epsilon_0'\tfrac{2}{3}\sin^2\theta \\ \epsilon''&=\epsilon_0'(3\sqrt{2}/2)\sin\theta\cos\theta \end{aligned} \tag{B2}$$

and ϵ_0, ϵ_0' are, as defined earlier,

$$\begin{aligned} \epsilon_0&=\tfrac{2}{3}D_u(s_{11}-s_{12})T \\ \epsilon_0'&=\tfrac{2}{3}D_u'(s_{44}/2)T \end{aligned} \tag{B3}$$

Employing a matrix representation[21] for J_x, J_y, and J_z, we get

$$H_e=\begin{bmatrix} \epsilon & (1/\sqrt{3})(1+i)\epsilon'' & (i/\sqrt{3})\epsilon' & 0 \\ (1/\sqrt{3})(1-i)\epsilon'' & -\epsilon & 0 & (i/\sqrt{3})\epsilon' \\ -(i/\sqrt{3})\epsilon' & 0 & -\epsilon & -(1/\sqrt{3})(1+i)\epsilon'' \\ 0 & -(i/\sqrt{3})\epsilon' & -(1/\sqrt{3})(1-i)\epsilon'' & \epsilon \end{bmatrix} \tag{B4}$$

Since we are interested in the masses for an arbitrary orientation of T in the $(1\bar{1}0)$ plane, we shall rotate the coordinate axes so k_3 is along T (it is not necessary to rotate J to change the axis of quantization). Choosing k_1 along the $[1\bar{1}0]$ direction as the axis of rotation, we make the transformation [see (A3)] from the crystal system to the stress coordinate system,

$$\begin{aligned} k_x&=\frac{1}{\sqrt{2}}k_1+\frac{1}{\sqrt{2}}k_2\cos\theta+\frac{1}{\sqrt{2}}k_3\sin\theta, \\ k_y&=-\frac{1}{\sqrt{2}}k_1+\frac{1}{\sqrt{2}}k_2\cos\theta+\frac{1}{\sqrt{2}}k_3\sin\theta, \\ k_z&=-k_2\sin\theta+k_3\cos\theta, \end{aligned} \tag{B5}$$

in which θ is the polar angle between k_z and k_3. This particular choice of 1, 2, 3 coordinates is advantageous because they automatically coincide with the principal axes of the mass tensor.

Direct substitution of (B5) into (7) to obtain the transformed $\mathbf{k}\cdot\mathbf{p}$ Hamiltonian is extremely tedious and, in fact, unnecessary. We can, instead, determine the masses m_1, m_2, and m_3 by diagonalizing the Hamiltonian for specific directions in k space, i.e., k_1, k_2, and k_3 successively.

If we set $k_2=k_3=0$, then the transformed Hamil-

[37] See, for example, C. Kittel, *Introduction to Solid-State Physics* (John Wiley & Sons, Inc., New York, 1957), p. 91. The compliance tensor (A7) differs from Kittel's set of compliance constants by a factor of $\frac{1}{4}$ before the s_{44}. This occurs because the set derived by Kittel is not a tensor since it was obtained using the conventional strain components which are, by definition, not tensor components. It was the failure to recognize this fact which led to the incorrect value of ϵ_0' given in reference 11.

tonian is

$$H_0(k_1)=\begin{bmatrix} (A+\frac{1}{2}B)k_1^2+\epsilon & (1/\sqrt{3})(1+i)\epsilon'' & (i/\sqrt{3})(\frac{1}{2}Nk_1^2+\epsilon') & 0 \\ (1/\sqrt{3})(1-i)\epsilon'' & (A-\frac{1}{2}B)k_1^2-\epsilon & 0 & (i/\sqrt{3})(\frac{1}{2}Nk_1^2+\epsilon') \\ -(i/\sqrt{3})(\frac{1}{2}Nk_1^2-\epsilon') & 0 & (A-\frac{1}{2}B)k_1^2-\epsilon & -(1/\sqrt{3})(1+i)\epsilon'' \\ 0 & -(i/\sqrt{3})(\frac{1}{2}Nk_1^2+\epsilon') & -(1/\sqrt{3})(1-i)\epsilon'' & (A+\frac{1}{2}B)k_1^2+\epsilon \end{bmatrix}. \quad \text{(B6)}$$

This can be exactly diagonalized. The eigenvalues of $H_0(k_1)$ are

$$E(k_1)=Ak_1^2\pm\tfrac{1}{2}[(B^2+\tfrac{1}{3}N)k_1^4+4(\epsilon B+\tfrac{1}{3}\epsilon' N)k_1^2 +4(\epsilon^2+\tfrac{1}{3}\epsilon'^2+\tfrac{2}{3}\epsilon''^2)]^{1/2}. \quad \text{(B7)}$$

Since we are only concerned with the bands near $\mathbf{k}=0$, we can neglect the k_1^4 terms which are small compared to the k_1^2 terms if the bands are well decoupled, i.e., $\epsilon, \epsilon' \gg Nk_1^2, Bk_1^2$; then

$$E(k_1)=Ak_1^2\pm[(\epsilon B+\tfrac{1}{3}\epsilon' N)k_1^2+\epsilon^2+\tfrac{1}{3}\epsilon'^2+\tfrac{2}{3}\epsilon''^2]^{1/2}. \quad \text{(B8)}$$

Expanding for small k_1 we get

$$E(k_1)=\left[A\pm\tfrac{1}{2}B\frac{\epsilon}{|\epsilon|}c_1(\theta)+\tfrac{1}{2}N\frac{\epsilon'}{|\epsilon'|}c_2(\theta)\right]k_1^2 \pm(\epsilon^2+\tfrac{1}{3}\epsilon'^2+\tfrac{2}{3}\epsilon''^2)^{1/2}, \quad \text{(B9)}$$

where

$$c_1(\theta)=(1/D)(\cos^2\theta-\tfrac{1}{2}\sin^2\theta), \qquad c_2(\theta)=(1/2D)|\beta|\sin^2\theta, \quad \text{(B10)}$$

in which

$$D(\theta)=[(\tfrac{1}{2}\sin^2\theta-\cos^2\theta)^2+\tfrac{3}{4}\beta^2\sin^2\theta(1+3\cos^2\theta)]^{1/2}, \quad \text{(B11)}$$

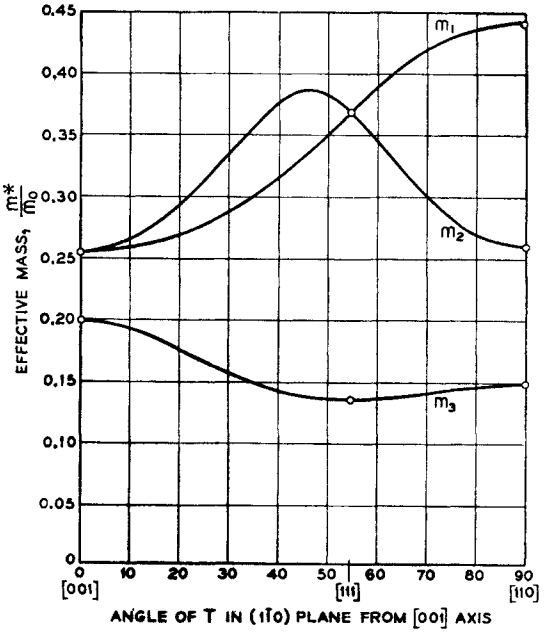

FIG. 17. The anisotropy of the effective masses for the "upper" hole band $E_{1/2}^+$ for uniaxially compressed silicon with respect to the direction of T in the $(1\bar{1}0)$ plane. The curves were calculated using the values of A, B, N, and β given in Table III. The experimental points are shown.

and $\beta=\epsilon_0'/\epsilon_0$ is the splitting anisotropy parameter. The upper and lower signs always refer, respectively, to the "top" and "bottom" $J=\frac{3}{2}$ bands.

The same process can be repeated for the remaining directions k_2 and k_3. Next, letting $k_1=k_3=0$, we obtain to lowest order in k_2,

$$E(k_2)=\left[A\pm\tfrac{1}{2}B\frac{\epsilon_0}{|\epsilon_0|}c_3(\theta)\pm\tfrac{1}{2}N\frac{\epsilon_0'}{|\epsilon_0'|}c_4(\theta)\right]k_2^2 \pm(\epsilon^2+\tfrac{1}{3}\epsilon'^2+\tfrac{2}{3}\epsilon''^2)^{1/2}, \quad \text{(B12)}$$

where

$$c_3(\theta)=(1/D)(\cos^2\theta-\tfrac{1}{2}\sin^2\theta)(\cos^2\theta-2\sin^2\theta), \qquad c_4(\theta)=(3/2D)|\beta|\cos^2\theta\sin^2\theta. \quad \text{(B13)}$$

Finally, if we set $k_1=k_2=0$, we get

$$E(k_3)=\left[A\pm\tfrac{1}{2}B\frac{\epsilon_0}{|\epsilon_0|}c_5(\theta)\mp\tfrac{1}{2}N\frac{\epsilon_0'}{|\epsilon_0'|}c_5(\theta)\right]k_3^2 \pm[\epsilon^2+\tfrac{1}{3}\epsilon'^2+\tfrac{2}{3}\epsilon''^2]^{1/2}, \quad \text{(B14)}$$

where

$$c_5(\theta)=(1/D)(\cos^2\theta-\tfrac{1}{2}\sin^2\theta)(\sin^2\theta-2\cos^2\theta), \qquad c_6(\theta)=(1/2D)|\beta|\sin^2\theta(3\cos^2\theta+1). \quad \text{(B15)}$$

2. *Band Splitting* Δ

From the foregoing the anisotropic energy splitting Δ for the $J=\frac{3}{2}$ valence bands is

$$\Delta=2(\epsilon^2+\tfrac{1}{3}\epsilon'^2+\tfrac{2}{3}\epsilon''^2)^{1/2}. \quad \text{(B16)}$$

Expressed explicitly in terms of the angle θ, this becomes

$$\Delta=2|\epsilon_0|D(\theta). \quad \text{(B17)}$$

For $\beta=1$ we find that $D(\theta)\equiv 1$ and the splitting becomes isotropic, $\Delta=2|\epsilon_0|$.

3. *Anisotropy of the Effective Masses with respect to T*

At this point it is perhaps worthwhile to summarize the behavior of the three hole effective masses m_1, m_2, and m_3 in strained silicon by exhibiting their complete anisotropies as T is rotated in the $(1\bar{1}0)$ plane. Using the values of A, B, N, and β in Table III we calculate these anisotropies from Eqs. (B9)–(B15). In Fig. 17 are shown the curves thus obtained upon which are superimposed the experimental points for the masses at the three principal crystallographic directions. For the high-symmetry directions [001] and [111] the unique nature of the energy ellipsoids, i.e., axial symmetry, is clearly evident.

The large anisotropies of the mass with respect to T suggests that, in principal, greater over-all accuracy could be achieved in determining the band parameters by measuring the masses for additional stress directions and then employing appropriate curve-fitting techniques. In view of the complications brought about by the mass dependence on strain, however, the extra effort in pursuing this approach does not seem presently justifiable.

C. Corrections for Small Misorientations of T from [111]

It is often difficult to align the direction of the applied stress precisely along the desired crystallographic direction. Since the effective masses are extrema for $T\|[001]$ and $T\|[110]$, a small misalignment of T by $\Delta\theta$ from these directions is usually not serious, introducing into the measurements an error of order $(\Delta\theta)^2$. However, for T near [111] where the effective masses are changing with direction of T a significant error of first order in $\Delta\theta$ is possible. We calculate here these first-order changes in the cyclotron mass for the [111] case to enable one to make corrections for the inevitable small experimental misorientations.

In the present experimental setup using flat samples out in the $(1\bar{1}0)$ plane, the misorientations are confined almost entirely to this same plane. Consequently, we can utilize the results of Sec. B and calculate the changes of mass with respect to the polar angle θ. Differentiating the inverse effective masses with respect to θ and evaluating the derivatives for the [111] direction, we get

$$\begin{aligned}
\Delta\left(\frac{1}{m_1}\right)&=\pm\sqrt{2}\left(\frac{N}{6}\frac{\epsilon_0'}{|\epsilon_0'|}-\frac{1}{|\beta|}\frac{B}{2}\frac{\epsilon_0}{|\epsilon_0|}\right)\Delta\theta,\\
\Delta\left(\frac{1}{m_2}\right)&=\mp\sqrt{2}\left(\frac{N}{6}\frac{\epsilon_0'}{|\epsilon_0'|}-\frac{1}{|\beta|}\frac{B}{2}\frac{\epsilon_0}{|\epsilon_0|}\right)\Delta\theta,\\
\Delta\left(\frac{1}{m_3}\right)&=0,
\end{aligned}\tag{C1}$$

where the upper and lower signs refer to the "top" and "bottom" $J=\frac{3}{2}$ bands, respectively (B and N are in units of $\hbar^2/2m_0$). If we add the above deviations to the zeroth order masses $m_\perp'$ and $m_{\|}'$ for $T\|[111]$, we can write the three total effective masses as

$$\begin{aligned}
m_1&=m_\perp'(1\mp\delta),\\
m_2&=m_\perp'(1\pm\delta),\\
m_3&=m_{\|}',
\end{aligned}\tag{C2}$$

where

$$\delta=\left[\sqrt{2}\left(\frac{N}{6}\frac{\epsilon_0'}{|\epsilon_0'|}-\frac{1}{|\beta|}\frac{B}{2}\frac{\epsilon_0}{|\epsilon_0|}\right)\Big/\times\left(A\pm\frac{N}{6}\frac{\epsilon_0'}{|\epsilon_0'|}\right)\right]\Delta\theta.\tag{C3}$$

It is worth noting that m_3 reaches an extremum for $T\|[111]$, whereas m_1 and m_2 cross the [111] direction with equal but opposite slopes (see Fig. 17).

The anisotropy of the cyclotron effective mass in the $(1\bar{1}0)$ plane is given by

$$m^*=\left(\frac{\cos^2\varphi}{m_1m_2}+\frac{\sin^2\varphi}{m_1m_3}\right)^{-1/2},\tag{C4}$$

where φ is the angle between H_0 and the stress direction. Using the masses m_1, m_2, and m_3 from (C2) we obtain

$$m^*=m_0^*\left(1\mp\frac{m_0^{*2}}{m_\perp'm_{\|}'}\frac{\delta}{2}\sin^2\varphi\right),\tag{C5}$$

where m_0^* is the anisotropic cyclotron effective mass for $T\|[111]$

$$m_0^*=\left(\frac{\cos^2\varphi}{m_\perp'^2}+\frac{\sin^2\varphi}{m_\perp'm_{\|}'}\right)^{-1/2}.\tag{C6}$$

For $H_0\|T$ the correction is zero; however, for $\varphi=90°$ the mass shift is nearly maximum

$$\Delta m^*/m_0^*=\mp\tfrac{1}{2}\delta\sim\pm0.3\Delta\theta,$$

which represents a $\frac{1}{2}\%$ correction for a 1° misorientation.

D. Anisotropy of the Linear Mass Shift Parameters

Hasegawa[10] has pointed out that the measured inverse effective masses for the decoupled valence bands of silicon have the following form for the axially symmetric cases $T\|[001]$ and $T\|[111]$,

$$\begin{aligned}
\frac{1}{(m_\perp)_{\text{meas}}}&=\frac{1}{m_\perp}+\alpha_\perp T,\\
\frac{1}{(m_{\|})_{\text{meas}}}&=\frac{1}{m_{\|}}+\alpha_{\|}T
\end{aligned}\tag{D1}$$

(assuming the γ/T component has been extracted). Here $\alpha_\perp$ and $\alpha_{\|}$ are the linear effective-mass shift parameters and $m_\perp$ and $m_{\|}$ are the "zero strain" masses defined in Sec. II. As a rule $(m_\perp)_{\text{meas}}$ and $(m_{\|})_{\text{meas}}$ cannot be determined directly but must be ascertained from the anisotropy of the cyclotron effective mass,

$$m^*(\varphi)=\left[\frac{\cos^2\varphi}{(m_\perp)_{\text{meas}}^2}+\frac{\sin^2\varphi}{(m_\perp m_{\|})_{\text{meas}}}\right]^{-1/2},\tag{D2}$$

where φ is the angle between H_0 and the symmetry axis of the ellipsoid. In addition, we should like as well to determine $\alpha_\perp$ and $\alpha_{\|}$ in a similar way from the anisotropy of the linear effective-mass shifts described

by $\alpha(\varphi)$ according to

$$\frac{1}{m^*(\varphi)}=\frac{1}{m_0^*(\varphi)}+\alpha(\varphi)T. \tag{D3}$$

The requisite relation for $\alpha(\varphi)$ in terms of $\alpha_\perp$ and $\alpha_{||}$ can be obtained as follows: If we substitute Eq. (D1) into Eq. (D2) and expand to first order in T, we obtain, after identifying the resulting terms with those in Eq. (D3), the zeroth-order effective-mass anisotropy

$$m_0^*(\varphi)=\left(\frac{\cos^2\varphi}{m_\perp^2}+\frac{\sin^2\varphi}{m_\perp m_{||}}\right)^{-1/2}, \tag{D4}$$

as expected and, in addition, the first-order term containing the anisotropy for $\alpha(\varphi)$,

$$\alpha(\varphi)=\tfrac{1}{2}m_0^*(\varphi)\left[\frac{2\alpha_\perp}{m_\perp}\cos^2\varphi+\left(\frac{\alpha_\perp}{m_{||}}+\frac{\alpha_{||}}{m_\perp}\right)\sin^2\varphi\right]. \tag{D5}$$

The same analysis obtains for the case $T\|[110]$ for which there are *three* different inverse effective masses

$$\begin{aligned}\frac{1}{(m_1)_{\text{meas}}}&=\frac{1}{m_1}+\alpha_1 T,\\ \frac{1}{(m_2)_{\text{meas}}}&=\frac{1}{m_2}+\alpha_2 T,\\ \frac{1}{(m_3)_{\text{meas}}}&=\frac{1}{m_3}+\alpha_3 T,\end{aligned} \tag{D6}$$

where 1, 2, and 3 are along the $[1\bar{1}0]$, $[00\bar{1}]$, and $[110]$ axes, respectively. The effective masses m_1, m_2, and m_3 are those given by Eq. (25) in Sec. II; the effective-mass shift constants α_1, α_2, and α_3 for $T\|[110]$ have been determined by Hasegawa.[22] We find that the zeroth-order mass anisotropies in each of the principal planes are

$$\begin{aligned}m_0^*(001)&=\left(\frac{\cos^2\varphi_1}{m_2m_3}+\frac{\sin^2\varphi_1}{m_1m_2}\right)^{-1/2},\\ m_0^*(110)&=\left(\frac{\cos^2\varphi_2}{m_1m_3}+\frac{\sin^2\varphi_2}{m_2m_3}\right)^{-1/2},\\ m_0^*(1\bar{1}0)&=\left(\frac{\cos^2\varphi_3}{m_1m_2}+\frac{\sin^2\varphi_3}{m_1m_3}\right)^{-1/2},\end{aligned} \tag{D7}$$

where φ_1, φ_2, and φ_3 are the angles between H_0 and the 1, 2, and 3 axes, respectively. The anisotropies for α in these same planes are

$$\begin{aligned}\alpha(00\bar{1})&=\tfrac{1}{2}m_0^*(00\bar{1})(X\cos^2\varphi_1+Y\sin^2\varphi_1),\\ \alpha(110)&=\tfrac{1}{2}m_0^*(110)(Y\cos^2\varphi_2+Z\sin^2\varphi_2),\\ \alpha(1\bar{1}0)&=\tfrac{1}{2}m_0^*(1\bar{1}0)(Z\cos^2\varphi_3+X\sin^2\varphi_3).\end{aligned} \tag{D8}$$

Here we have defined

$$\begin{aligned}X&=\alpha_1/m_2+\alpha_2/m_1,\\ Y&=\alpha_2/m_3+\alpha_3/m_2,\\ Z&=\alpha_3/m_1+\alpha_1/m_3.\end{aligned} \tag{D9}$$

In order to obtain α_1, α_2 and α_3 from the measured anisotropies it is useful to have the inverse relations

$$\begin{aligned}\alpha_1&=\frac{1}{2}\left(m_2X+m_3Z-\frac{m_2m_3}{m_1}Y\right),\\ \alpha_2&=\frac{1}{2}\left(m_3Y+m_1X-\frac{m_3m_1}{m_2}Z\right),\\ \alpha_3&=\frac{1}{2}\left(m_1Z+m_2Y-\frac{m_1m_2}{m_3}X\right).\end{aligned} \tag{D10}$$

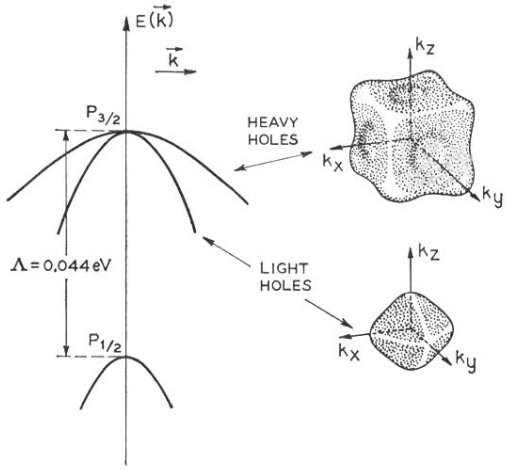

FIG. 1. The valence bands of "cubic" silicon near $\mathbf{k}=0$. The warped energy surfaces of the light- and heavy-hole bands are shown schematically. The spin-orbit split-off band labeled by its spectroscopic character $p_{1/2}$ has spherical energy surfaces which are not shown.

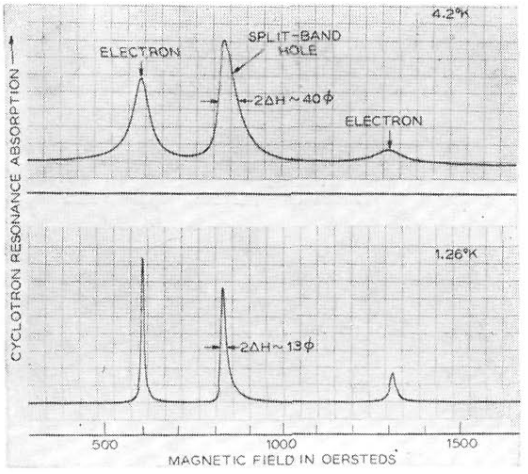

FIG. 13. Comparison of cyclotron resonance lines in uniaxially stresses silicon at 1.26 and 4.2°K. The traces were taken for H_0 and $T\|[001]$ ($T=2550$ kg/cm^2) and $\nu\approx 8800$ Mc/sec.

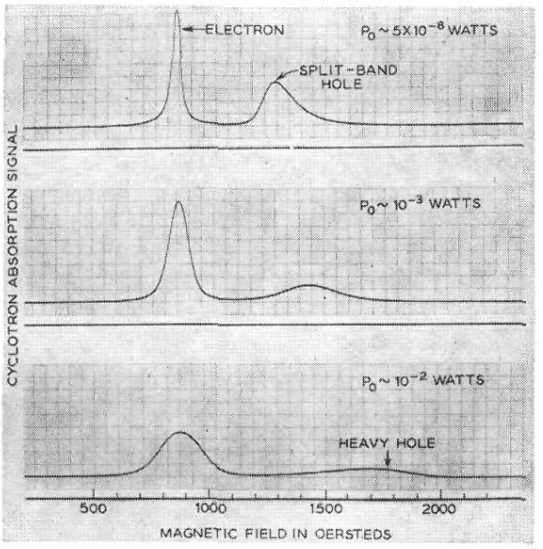

FIG. 15. The effects of microwave carrier heating upon the cyclotron resonance lines in uniaxially stressed silicon. The traces were taken for H_0 and $T \| [111]$ ($T \approx 1000$ kg/cm^2), 1.26°K, and $\nu \approx 8900$ Mc/sec. In (c) the high microwave electric fields ($E_1 \approx 10$ V/cm) shift the split-band hole line nearly to the position indicated for the unstressed "heavy" hole line. The electron lines are severely broadened by the microwave carrier heating at the power levels 10^{-3} to 10^{-2} W in (b) and (c).

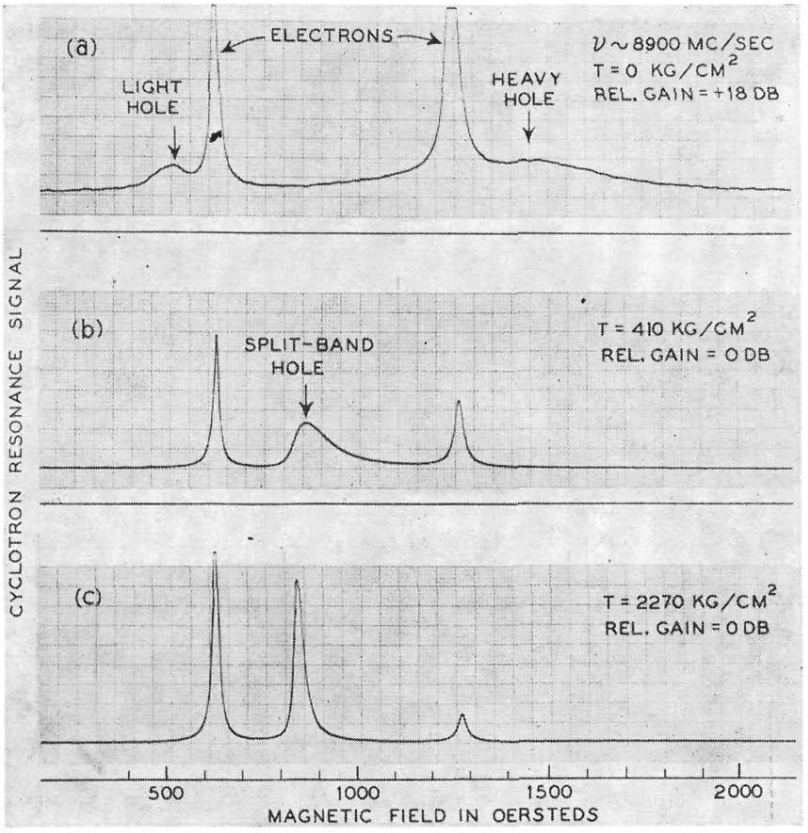

FIG. 3. The behavior of the cyclotron resonance lines in silicon as a uniaxial, compressive stress is applied along the [001] axis. The recorder traces were taken at 1.26°K and $\nu \approx 8900$ Mc/sec with H_0 in the $(1\bar{1}0)$ plane and inclined 15° from the [001] axis. The broad, weak lines of the unstrained "classical" hole resonances in (a) point up the difficulties mentioned in Sec. II in obtaining accurate measurements of their effective masses.